

RX J0513.9–6951: THE FIRST EXAMPLE OF ACCRETION WIND EVOLUTION, A KEY EVOLUTIONARY PROCESS TO TYPE Ia SUPERNOVAE

IZUMI HACHISU

Department of Earth Science and Astronomy, College of Arts and Sciences, University of Tokyo, Komaba,
 Meguro-ku, Tokyo 153-8902, Japan
 hachisu@chianti.c.u-tokyo.ac.jp

AND

MARIKO KATO

Department of Astronomy, Keio University, Hiyoshi, Kouhoku-ku, Yokohama 223-8521, Japan
 mariko@educ.cc.keio.ac.jp

to appear in the Astrophysical Journal

ABSTRACT

A new self-sustained model for long-term light curve variations of RX J0513.9–6951 is proposed based on an optically thick wind model of mass-accreting white dwarfs (WDs). When the mass accretion rate to a WD exceeds the critical rate of $\sim 1 \times 10^{-6} M_{\odot} \text{ yr}^{-1}$, optically thick strong winds begin to blow from the WD so that a formation of common envelope is avoided. The WD can accrete and burn hydrogen-rich matter atop the WD at the critical rate. The excess matter transferred to the WD above the critical rate is expelled by winds. This is called the accretion wind evolution. This ejection process, however, occurs intermittently because the mass transfer is attenuated by strong winds: the strong winds collide with the secondary surface and strip off the very surface layer of the secondary. The matter stripped-off is lost from the binary system. Properly formulating this mass stripping effect and the ensuing decay of mass transfer rate, we are able to reproduce, in a self-sustained manner, the transition between the optical high/X-ray off and optical low/X-ray on states of RX J0513.9–6951. Thus RX J0513.9–6951 is the first example of the accretion wind evolution, which is a key evolutionary process in a recently developed evolutionary path to Type Ia supernovae.

Subject headings: binaries: close — novae, cataclysmic variables — stars: individual
 (RX J0513.9–6951) — stars: winds, outflows — X-rays: stars

1. INTRODUCTION

The Large Magellanic Cloud (LMC) transient supersoft X-ray source RX J0513.9–6951 (hereafter RX J0513) was discovered by ROSAT (Schaeidt et al. 1993) and has been extensively observed (e.g., Reinsch et al. 2000, for recent progress). Soon after the X-ray discovery, it was optically identified as a binary with an orbital period of 0.76 days (Pakull et al. 1993). Its remarkable observational features are summarized as follows: (1) Optical monitoring of RX J0513 shows quasi-regular transitions between high ($V \sim 16.6$) and low ($V \sim 17.4$) states (Alcock et al. 1996). (2) The duration of the optical high state is ~ 60 –150 days while the low states last for ~ 40 days (see, e.g., Fig. 1 of Cowley et al. 2002, for recent observational summary). (3) Copious supersoft X-rays (~ 30 –40 eV) were detected only in the optical low state (e.g., Schaeidt et al. 1993; Reinsch et al. 1996; Southwell et al. 1996). (4) The transitions between X-ray off and on are very rapid, in about one day or so, while the optical transitions from high to low occurs in several days (e.g., Reinsch et al. 2000). The transition mechanism between high and low states has not been fully elucidated yet, although a few ideas were proposed so far (see, e.g., Reinsch et al. 2000, for a recent progress).

Very recently, based on an optically thick wind model of mass-accreting white dwarfs (WDs), Hachisu & Kato (2003) have proposed a new transition mechanism between optical high/X-ray off and optical low/X-ray on states.

They first modeled light curves of the 2000 outburst of the recurrent nova CI Aql and then showed that the size of a disk around the WD expands largely up to the companion star or over in a strong wind phase. Including this effect of disk expansion in the strong wind phase, they have reproduced a sharp ~ 1 mag rise in the optical light curve of RX J0513. This is the optical high/X-ray off state, because the optically thick winds of WDs certainly obscure supersoft X-rays. On the other hand, it drops sharply by a magnitude when the wind stops because the size of the disk returns to its original size. This is the optical low/X-ray on state. However, Hachisu & Kato (2003) gave only a simple outline of their mechanism without detailed physical descriptions. In this paper, we propose a full description of the mechanism and calculate light curves for various conditions. We are able to reproduce basic features of the observed light curves by this new mechanism.

It has been frequently discussed that supersoft X-ray sources (SSSs) are progenitors of Type Ia supernovae (SNe Ia). One of the promising evolutionary models to SNe Ia has been proposed by Hachisu, Kato, & Nomoto (1996). They theoretically found that mass accreting WDs blow strong winds when the mass accretion to the WD exceeds a critical rate, i.e., $\dot{M}_{\text{acc}} > \dot{M}_{\text{cr}} \sim 1 \times 10^{-6} M_{\odot} \text{ yr}^{-1}$. The so-called common envelope evolution does not occur (see Hachisu & Kato 2001, for a recent summary). The WD accretes hydrogen-rich matter and burns it atop the WD at the critical rate of \dot{M}_{cr} . The excess matter transferred above the critical rate is expelled by winds, i.e.,

$\dot{M}_{\text{wind}} = \dot{M}_{\text{acc}} - \dot{M}_{\text{cr}}$. In such a situation, the WD can grow up to near the Chandrasekhar mass (and eventually explode as an SN Ia). This is called the accretion wind evolution (Hachisu 2002; Hachisu & Kato 2001) against the common envelope evolution (Iben & Tutukov 1984; Webbink 1984). Thus, the accretion wind evolution is a key evolutionary process to produce Type Ia supernovae.

Binary systems in the accretion wind evolution are predicted to exist but no such systems have been identified yet. Here, we have reached the conclusion that RX J0513.9–6951 is the first example just in the accretion wind evolution, i.e., in the way to an SN Ia, the reason of which will be discussed below. A brief summary follows: The wind ejection process occurs not continuously but intermittently because the mass transfer is attenuated by the strong wind itself.

In §2, an outline of our basic model of RX J0513 is briefly introduced and summarized. Our new mechanism of transition between the optical high and low states, in which the mass transfer rate is attenuated by winds, is formulated in §3. A limit cycle model is given in §4 for RX J0513 long-term light curve variations. Discussion and conclusions follow in §5 and §6, respectively.

2. BRIEF DESCRIPTION OF A LIMIT CYCLE MODEL

Long-term variations in the optical light curves of RX J0513.9–6951 are considered as a limit cycle (e.g., Reinsch et al. 2000). Before going to detailed descriptions, we here give a rough sketch on our new mechanism. We adopt a binary system consisting of a WD, a disk around the WD, and a lobe-filling main-sequence (MS) companion, as illustrated in Figure 1. A circular orbit is assumed.

An essential thing is that WDs blow an optically thick, strong wind when the mass accretion rate to the WD exceeds the critical rate, i.e., $\dot{M}_{\text{acc}} > \dot{M}_{\text{cr}} \sim 1 \times 10^{-6} M_{\odot} \text{ yr}^{-1}$. If the MS companion is $\sim 2 - 3 M_{\odot}$, the mass transfer rate from the MS, \dot{M}_{MS} , is as large as a few times $10^{-6} M_{\odot} \text{ yr}^{-1}$ or more (e.g., Li & van den Heuvel 1997). We distinguish \dot{M}_{MS} from \dot{M}_{acc} because $\dot{M}_{\text{MS}} \neq \dot{M}_{\text{acc}}$ in some cases mentioned below.

Time-evolution of our limit cycle model is schematically summarized in Figure 2 (see also Hachisu & Kato 2003). A rapid mass accretion to the WD begins at A in Figure 2. The mass of the WD envelope rapidly increases and the WD envelope expands to blow an optically thick, strong wind. The strong wind causes a quick rise of V -mag at B, because the disk expands to a few to several times the previous size, that is, the disk expands from configuration (c) to configuration (a) in Figure 1. Because the disk is the main source in the optical light due to its irradiation effect, this expansion of the disk area causes a magnitude rise in the optical light. The massive winds having the rate of $\dot{M}_{\text{wind}} \sim 1 \times 10^{-6} M_{\odot} \text{ yr}^{-1}$ certainly absorb supersoft X-rays. Thus, this phase is the optical high and X-ray off state. As the WD photosphere expands further during the rapid mass accretion phase, optical brightness increases further from B to C even if the disk shape does not change in the wind phase.

The strong wind hits the MS companion and then strips-off its very surface layer. The gas stripped-off is lost from the binary. Therefore, the rapid mass accretion is sup-

pressed by the strong wind itself. The mass-stripping rate is roughly proportional to the wind mass loss rate. As the wind mass loss rate increases, the mass-stripping rate eventually overcomes the mass transfer rate. This happens at C'. However, the accretion disk still continues to supply mass to the WD at least during the viscous timescale of the accretion disk, t_{vis} . Then, mass accretion to the WD stops at C about t_{vis} after the mass transfer from the MS stops.

The mass of the WD envelope is now gradually decreasing due mainly to wind mass loss. The photosphere of the WD is also gradually shrinking. This makes a gradual decay of the optical light curve even if the disk shape is the same. The wind eventually stops at D. We expect copious supersoft X-rays after the wind stops. The disk shrinks to a normal size at E, that is, from configuration (a) to configuration (b) in Figure 1. This causes a sharp ~ 1 mag drop in the optical light. A rapid mass transfer from the MS to the disk resumes at E, and then the disk edge flares up at F, that is, configuration (b) to configuration (c) in Figure 1. It takes several dynamical timescales to change from E to F. This phase corresponds to the optical low and X-ray on state.

Because mass accretes to the WD via an accretion disk, this rapid mass accretion flow reaches the WD surface at G(=A) about t_{vis} after the rapid mass transfer from the MS resumes. Thus, the cycle is repeated.

3. THE BINARY MODEL

3.1. Basic Parameters of the Binary

A relatively massive white dwarf is suggested because of a rapid contraction timescale of the WD photosphere during the transition from optical high to low states (e.g., Southwell et al. 1996). We have adopted $M_{\text{WD}} = 1.3 M_{\odot}$ after Hachisu & Kato (2003) but later examined other cases of the WD mass, i.e., $M_{\text{WD}} = 1.35 M_{\odot}$, $1.2 M_{\odot}$, and $1.1 M_{\odot}$. Since the LMC metallicity is reported to be about a third of the solar metallicity, we assume the metallicity of $Z = 0.004$ and hydrogen content of $X = 0.7$ for the envelope of the WD. The mass ratio is assumed to be $q = M_{\text{MS}}/M_{\text{WD}} = 2$ because mass transfer occurs on a thermal timescale and a rate of $\dot{M}_{\text{MS}} \gtrsim 10^{-6} M_{\odot} \text{ yr}^{-1}$ is suggested by Southwell et al. (1996). Then, the companion mass is $M_{\text{MS}} = 2.6 M_{\odot}$ for $M_{\text{WD}} = 1.3 M_{\odot}$. The non-irradiated surface temperature of the lobe-filling $2.6 M_{\odot}$ MS companion is 13,000 K for the metallicity of $Z = 0.004$ (e.g., Fagotto et al. 1994).

For the orbital period of $P_{\text{orb}} = 0.763$ days (see below), the separation is $a = 5.53 R_{\odot}$, the radii of the effective Roche lobes are $R_1^* = 1.77 R_{\odot}$ for the primary (WD) and $R_2 = R_2^* = 2.43 R_{\odot}$ for the secondary (MS) component. The radius of a $2.6 M_{\odot}$ zero-age main-sequence (ZAMS) star is $R_{\text{ZAMS}} = 1.5 R_{\odot}$ for $Z = 0.004$, so that the secondary has already evolved to expand but still remains at the main-sequence (before exhaustion of central hydrogen).

The ephemeris of RX J0513 has been revised by Cowley et al. (2002) as

$$t(\text{JD}) = 2,448,858.099 + 0.7629434 \times E \quad (1)$$

at minima of the optical orbital modulations. We use this revised ephemeris with the MS companion being in front

of the WD at minima (see also Fig. 5 of Hutchings et al. 2002). The inclination angle is not known but suggested to be low. Here we adopt $i = 10^\circ$. Calculated light curves are not so different among $i = 0^\circ - 35^\circ$ as shown later.

3.2. Time Evolution of the WD Envelope

Time evolution of the photospheric radius and temperature of the WD are calculated from Kato & Hachisu's (1994) optically thick wind solutions after Hachisu & Kato (2001), i.e.,

$$\frac{d}{dt}\Delta M_{\text{env}} = \dot{M}_{\text{acc}} - \dot{M}_{\text{nuc}} - \dot{M}_{\text{wind}}, \quad (2)$$

where ΔM_{env} is the hydrogen-rich envelope mass of the WD, \dot{M}_{acc} the mass accretion rate to the WD, \dot{M}_{nuc} the decreasing rate by nuclear burning, and \dot{M}_{wind} the wind mass loss rate of the WD. The nuclear burning rate \dot{M}_{nuc} , wind mass loss rate \dot{M}_{wind} , photospheric radius R_{ph} , photospheric temperature T_{ph} , and luminosity L_{ph} as well as the photospheric wind velocity v_{ph} , of the WD are all given as a function of the envelope mass (ΔM_{env}) in the wind solutions (Kato & Hachisu 1994; Hachisu & Kato 2001), i.e.,

$$\dot{M}_{\text{nuc}} = f_1(\Delta M_{\text{env}}, X, Z, M_{\text{WD}}), \quad (3)$$

$$\dot{M}_{\text{wind}} = f_2(\Delta M_{\text{env}}, X, Z, M_{\text{WD}}), \quad (4)$$

$$R_{\text{ph}} = f_3(\Delta M_{\text{env}}, X, Z, M_{\text{WD}}), \quad (5)$$

$$T_{\text{ph}} = f_4(\Delta M_{\text{env}}, X, Z, M_{\text{WD}}), \quad (6)$$

$$L_{\text{ph}} = f_5(\Delta M_{\text{env}}, X, Z, M_{\text{WD}}), \quad (7)$$

$$v_{\text{ph}} = f_6(\Delta M_{\text{env}}, X, Z, M_{\text{WD}}). \quad (8)$$

Given the mass accretion rate \dot{M}_{acc} and the initial envelope mass, we are able to follow the time evolutions of the envelope mass and then the radius and temperature (and also the luminosity) of the WD by integrating equation (2).

3.3. Optically Thick Strong Winds

Mass transfer in RX J0513 probably proceeds in a Kelvin-Helmholtz timescale of the MS companion (e.g., van den Heuvel et al. 1992), so that it is as large as $\dot{M}_{\text{MS}} \sim 1 \times 10^{-6} M_\odot \text{ yr}^{-1}$ or more. When the mass transfer rate, \dot{M}_{MS} , exceeds the critical rate, i.e.,

$$\dot{M}_{\text{MS}} > \dot{M}_{\text{cr}} \approx 0.75 \times 10^{-6} \left(\frac{M_{\text{WD}}}{M_\odot} - 0.4 \right) M_\odot \text{ yr}^{-1}, \quad (9)$$

the mass-accreting WD expands to blow optically thick winds (e.g., Hachisu et al. 1996) and the mass loss rate approximately given by

$$\dot{M}_{\text{wind}} \approx \dot{M}_{\text{MS}} - \dot{M}_{\text{cr}}, \quad (10)$$

when all the transferred matter accretes to the WD, i.e., $\dot{M}_{\text{acc}} = \dot{M}_{\text{MS}}$. Equation (9) is the same form as that for the solar metallicity ($Z = 0.02$), but valid even for a lower metallicity of $Z = 0.004$ (e.g., Hachisu & Kato 2001).

3.4. Mechanism of Intermittent Mass Accretion

When strong winds collide with the surface of the companion, the surface is shock-heated and ablated in the wind. We estimate the shock-heating by assuming that the velocity component normal to the surface is dissipated by shock and its kinetic energy is converted into the thermal energy of the surface layer. The very surface layer of the envelope expands to be easily ablated in the wind. We regard that gas is ablated and lost from L3 point (L3 is the outer Lagrange point near the MS companion) when the gas gets the same amount of thermal energy as the difference of the Roche potentials between the MS surface and L3 point. Then the mass stripping rate is given by

$$\frac{GM}{a} (\phi_{\text{L3}} - \phi_{\text{MS}}) \cdot \dot{M}_{\text{strip}} = \frac{1}{2} v^2 \dot{M}_{\text{wind}} \cdot \eta_{\text{eff}} \cdot g(q), \quad (11)$$

where $M = M_{\text{WD}} + M_{\text{MS}}$, a is the separation of the binary, ϕ_{MS} the Roche potential at the MS surface, ϕ_{L3} means the Roche potential at L3 point near the MS companion, both of which are normalized by GM/a , η_{eff} the efficiency of conversion from kinetic energy to thermal energy by shock, $g(q)$ is the geometrical factor of the MS surface hit by the wind including the dissipation effect (normal component of the wind velocity), and $g(q)$ is only a function of the mass ratio $q = M_{\text{MS}}/M_{\text{WD}}$ (see Hachisu, Kato, & Nomoto 1999a, for more details). Here we modified equation (21) of Hachisu et al. (1999a) to include the effect of Roche lobe overflow from L3 point. Then the stripping rate is estimated as

$$\dot{M}_{\text{strip}} = c_1 \dot{M}_{\text{wind}}, \quad (12)$$

where

$$c_1 \equiv \frac{\eta_{\text{eff}} \cdot g(q)}{\phi_{\text{L3}} - \phi_{\text{MS}}} \left(\frac{v^2 a}{2GM} \right). \quad (13)$$

The efficiency of conversion is assumed to be $\eta_{\text{eff}} = 1$. Then, we have

$$c_1 \approx 0.1 \left(\frac{v}{400 \text{ km s}^{-1}} \right)^2 \approx 10, \quad (14)$$

for the wind velocity of $v_{\text{wind}} = 3800 \text{ km s}^{-1}$ (e.g., Crampton et al. 1996; Hutchings et al. 2002; Southwell et al. 1996), $a = 5.5 R_\odot$, $M = 3.9 M_\odot$, $\phi_{\text{L3}} - \phi_{\text{MS}} = 0.3$, and $g(q) = 0.025$ for the mass ratio $q = M_{\text{MS}}/M_{\text{WD}} = 2$ (Hachisu et al. 1999a).

In such a wind phase, the net mass accretion rate to the WD, \dot{M}_{acc} , is modified as

$$\dot{M}_{\text{acc}} = \begin{cases} 0 \text{ (or } \epsilon), & \text{for } \dot{M}_{\text{MS}} \leq \dot{M}_{\text{strip}} \\ \dot{M}_{\text{MS}} - \dot{M}_{\text{strip}}, & \text{for } \dot{M}_{\text{MS}} > \dot{M}_{\text{strip}} \end{cases} \quad (15)$$

as illustrated in Figure 3. Here we adopt a small value of $\epsilon = 1 \times 10^{-7} M_\odot \text{ yr}^{-1}$ when $\dot{M}_{\text{MS}} < \dot{M}_{\text{strip}}$ because the mass accretion to the WD does not stop abruptly but probably continues at least for a draining time of the accretion disk. We do not know the exact draining time of the accretion disk after the mass transfer from the MS stops. Alternatively, we just assume a small rate of the mass accretion ϵ to mimic the draining of the disk during that $\dot{M}_{\text{MS}} < \dot{M}_{\text{strip}}$.

To know when the rapid mass accretion resumes, we monitor the upper level of flow in Figure 3 as

$$\frac{d}{dt} M_{\text{flow}} = \dot{M}_{\text{MS}} - \dot{M}_{\text{strip}} - \dot{M}_{\text{acc}}, \quad (16)$$

with the initial value of $M_{\text{flow}} = 0$. During that $\dot{M}_{\text{strip}} > \dot{M}_{\text{MS}}$, M_{flow} decreases to a large negative value as illustrated in Figure 3b. Then the mass transfer from the MS stops or its rate drops to ϵ . Once the mass accretion rate drops below the critical rate, i.e., $\dot{M}_{\text{acc}} < \dot{M}_{\text{cr}}$, the wind gradually weakens and eventually stops. The stripping effect vanishes ($\dot{M}_{\text{strip}} = 0$) and then the level of flow begins to rise. We start again the rapid mass accretion when the level reaches $M_{\text{flow}} = 0$ as illustrated in Figure 3a.

It should be noticed that equation (2) is on the WD but equations (11)–(16) are on the MS. Therefore, the mass accretion rate, \dot{M}_{acc} , may not be the same on each side at the specific time, t , because it takes a viscous timescale of the accretion disk for gas to reach the WD surface from the MS surface. Here we adopt a viscous timescale of

$$t_{\text{vis}} = \frac{R_{\text{disk}}^2}{\nu} = \frac{R_{\text{disk}}}{\alpha_{\text{vis}}} \frac{R_{\text{disk}}}{c_s H} \sim 40 \left(\frac{\alpha_{\text{vis}}}{0.1} \right)^{-1} \text{ days}, \quad (17)$$

where ν is the viscosity, α_{vis} the α parameter of Shakura & Sunyaev (1973), c_s the sound speed, and H the vertical height of the accretion disk. We adopt $R_{\text{disk}} = 1.4 R_{\odot}$ and $H/R_{\text{disk}} \sim 0.1$ for $T_{\text{disk}} \sim 30000 - 50000$ K and $c_s \sim 30 \text{ km s}^{-1}$. Then, we have

$$\dot{M}_{\text{acc}}(t) \Big|_{\text{WD}} = \dot{M}_{\text{acc}}(t - t_{\text{vis}}) \Big|_{\text{MS}}. \quad (18)$$

3.5. Irradiation Effects of Disk

The irradiation effects both of the disk and of the MS companion play an essential role in the light curve modeling. For the basic structure of the accretion disk, we assume an axi-symmetric structure with the size and thickness of

$$R_{\text{disk}} = \alpha R_1^*, \quad (19)$$

and

$$h = \beta R_{\text{disk}} \left(\frac{\varpi}{R_{\text{disk}}} \right)^{\nu}, \quad (20)$$

where R_{disk} is the outer edge of the accretion disk, R_1^* is the effective radius of the inner critical Roche lobe for the WD component, h is the height of the surface from the equatorial plane, and ϖ is the distance on the equatorial plane from the center of the WD. Such binary models are illustrated in Figure 1. We assume that the photosphere of the WD, the MS companion, and the accretion disk emit photons as a blackbody at a local temperature which varies with position.

We adopt $\nu = 1$ during the strong wind phases, i.e., configuration (a) in Figure 1 and just after the wind stops (but before a rapid mass transfer from the MS resumes), i.e., configuration (b) in Figure 1, but $\nu = 2$ in the no wind case, i.e., configuration (c) in Figure 1. This ϖ -square law mimics the effect of elevated rim of the accretion disk by spray as discussed by Schandl, Meyer-Hofmeister, & Meyer (1997) for luminous supersoft X-ray sources. On the other hand, we simply assume $\nu = 1$ in the wind phase, because such an elevated rim is blown in the wind during a strong wind phase. The efficiency of irradiation is assumed to be 0.5 both for the disk and for the companion (see also Schandl, Meyer-Hofmeister, & Meyer 1997; Meyer-Hofmeister, Schandl, & Meyer 1997).

The size and thickness of disk, α and β , are also the important parameters that determine the brightness of disk

by irradiation effects. Hachisu & Kato (2003) have determined α and β from the light curve fitting of CI Aql in outburst. The disk expands up to the companion star as shown in Figure 1a, i.e., $\alpha \sim 2 - 3$, because the disk surface is blown in the wind. It shrinks to a normal size of $\alpha = 0.7 - 0.8$ after the wind stops. These two parameters of (α, β) are determined as $(\alpha, \beta) = (3.0, 0.05) \rightarrow (0.8, 0.05) \rightarrow (0.8, 0.3)$, during the wind phase, just after the wind stops, and then the rapid mass transfer resumes, respectively (see Hachisu & Kato 2003, for more details). The shrink from a large, extended size to a normal size is important in the modeling of a sharp ~ 1 mag drop in the optical light curve. Thus, a large expansion of the disk in the strong wind phase has been first confirmed in the 2000 outburst of the recurrent nova CI Aql.

We find essentially the same sets of (α, β) as in Hachisu & Kato (2003) is valid for RX J0513. We may understand such a large expansion of the disk beyond the Roche lobe as follows: Observationally very fast winds have been reported, for example, 3800 km s^{-1} in RX J0513 (see, e.g., Crampton et al. 1996; Hutchings et al. 2002; Southwell et al. 1996). The wind mass loss rate is calculated to be $10^{-6} - 10^{-4} M_{\odot} \text{ yr}^{-1}$ in such a strong wind phase (e.g., Hachisu & Kato 2001). There is a large velocity difference between the wind and the disk surface. It certainly drives the Kelvin-Helmholtz instability at the interface, so that the very surface layer of the disk is dragged away outward with the velocity at least several hundred km s^{-1} , i.e., almost a free stream going outward. This surface free stream is initially optically thick at the original disk region but becomes optically thin somewhere outside because of geometrical dilution effect. Only the optically thick region of disk stream can contribute to the optical light by irradiation, so that we regard the radius of transition region between optically thick and thin as the edge of the disk. In this sense, the disk edge as shown in Figure 1a is not the boundary of matter but just a transition from optically thick to thin of the disk surface flow.

It should be noted that a high density part of the disk is hardly changed by this relatively tenuous surface free stream and resides in within its Roche lobe because the internal density of the disk is much denser than that of the WD wind. In the case of Figure 4, for example, the wind mass loss rate is about $1 \times 10^{-6} M_{\odot} \text{ yr}^{-1}$ and its velocity is $\sim 4000 \text{ km s}^{-1}$, so that the density of the wind is estimated from the continuity ($\dot{M}_{\text{wind}} = 4\pi r^2 \rho v$) to be about $10^{-11} \text{ g cm}^{-3}$ at the distance of $1 R_{\odot}$ from the center of the WD. On the other hand, the density of the standard accretion disk is about $10^{-1} \text{ g cm}^{-3}$ at the same radius. Here, we assume the standard accretion disk model (Shakura & Sunyaev 1973) with the mass accretion rate of $\sim 5 \times 10^{-6} M_{\odot} \text{ yr}^{-1}$.

It should be also addressed that optically thick winds are accelerated deep inside the photosphere ($\tau \gg 1$) but the wind itself becomes optically thin ($\tau \ll 1$) far above the WD photosphere as the definition of photosphere. Therefore, we do not expect any large optical contribution from the wind itself far outside the WD photosphere (see, e.g., Meyer-Hofmeister et al. 1997, for an estimation of small wind contributions to the optical light).

The numerical methods for obtaining light curves, including the above irradiation effects, have been described

in more detail in Hachisu & Kato (2001).

4. LIMIT CYCLE MODEL OF LONG-TERM VARIATIONS

4.1. A template light curve

Assuming $\dot{M}_{\text{MS}} = 5 \times 10^{-6} M_{\odot} \text{ yr}^{-1}$, $c_1 = 10.0$, and $t_{\text{vis}} = 20.5$ days, we have calculated time evolution of our binary system with the initial envelope mass of $\Delta M_{\text{env}} = 5 \times 10^{-7} M_{\odot}$. The obtained V -light curve and color (second panel), accretion rate (\dot{M}_{acc} on the WD) and wind mass loss rate in units of $10^{-6} M_{\odot} \text{ yr}^{-1}$ (third panel), radius (R_{\odot}) and temperature (eV) of the WD photosphere (bottom panel) together with the MACHO observation (top panel) are shown in Figure 4. Direct fitting to the observational light curves gives us an apparent distance modulus of $(m - M)_V = 18.7$. If we use the color excess of $E(B - V) = 0.13$ (Gänsicke et al. 1998), the distance to RX J0513 is $(m - M)_0 = 18.3$, being consistent with the relatively short distance to the LMC. In this paper, we use $(m - M)_V = 18.7$.

At the beginning of time-evolution calculations, the mass of the WD envelope is small so that the WD does not blow a wind yet. Its envelope mass increases because of $\dot{M}_{\text{MS}} = \dot{M}_{\text{acc}} > \dot{M}_{\text{nuc}}$ ($\dot{M}_{\text{wind}} = 0$). When the envelope mass reaches $\Delta M_{\text{env}} = 6.5 \times 10^{-7} M_{\odot}$, the WD photosphere expands to $R_{\text{ph}} = 0.087 R_{\odot}$ and begins to blow a wind. The disk size expands from $(\alpha, \beta) = (0.8, 0.2)$ to $(3.0, 0.05)$ in dynamical timescales. Here we adopt a few days as the transition time, because the strong winds easily blow the very surface layer of the disk in the wind. The wind mass loss rate is about $\dot{M}_{\text{wind}} = 1 \times 10^{-8} M_{\odot} \text{ yr}^{-1}$ only one day after the wind starts, which is large enough to completely obscure soft X-rays (see, e.g., discussion of Southwell et al. 1996). The occurrence of optically thick winds can naturally explain the very rapid emergence and decay ($\lesssim 1 - 2$ days) of supersoft X-rays accompanied by the transition between the optical high and low states (Reinsch et al. 2000). We discuss again in more detail this transition timescale of soft X-rays below in §5.

The envelope mass continues to increase and the wind mass loss rate also grows. The WD photosphere also continues to expand and this causes a gradual increase in the optical light curve. The mass transfer from the MS is suppressed when the wind mass loss rate reaches $\dot{M}_{\text{wind}} = 0.5 \times 10^{-6} M_{\odot} \text{ yr}^{-1}$, because $\dot{M}_{\text{strip}} = 10 \dot{M}_{\text{wind}} = \dot{M}_{\text{MS}} = 5.0 \times 10^{-6} M_{\odot} \text{ yr}^{-1}$. However, the mass accretion to the WD still continues at a high rate and the wind mass loss rate reaches $\dot{M}_{\text{wind}} = 1.0 \times 10^{-6} M_{\odot} \text{ yr}^{-1}$ as shown in Figure 4, because the mass in the accretion disk is drained to the WD in another 20.5 days of t_{vis} time delay. The mass accretion to the WD eventually stops and the mass of the WD envelope begins to decrease due to wind mass loss and nuclear burning. The WD photosphere gradually shrinks from $R_{\text{WD,ph}} = 0.24 R_{\odot}$ to $0.087 R_{\odot}$ during the wind phase. This causes the gradual decrease in the optical light curve until the end of high state. When the mass of the WD envelope decreases to $\Delta M_{\text{env}} = 6.5 \times 10^{-7} M_{\odot}$, the wind stops.

The WD photosphere begins to shrink quickly after the wind stops. It takes 34 days to collapse from $0.087 R_{\odot}$ to $0.03 R_{\odot}$. The photospheric temperature increases quickly from 30 eV to 40 eV during this period, which is very con-

sistent with the blackbody temperature of supersoft X-rays (Schaeidt et al. 1993). When the wind stops, the wind mass loss rate decreases from $\dot{M}_{\text{wind}} = 1.0 \times 10^{-8} M_{\odot} \text{ yr}^{-1}$ to zero in a day. This is again very consistent with a sharp emergence of supersoft X-rays (about a day or so, see Reinsch et al. 2000).

In Figure 3, during the strong wind phase the schematic mass flow goes to much below the level of full. After the wind stops, it gradually goes up and eventually reaches the level of full. It takes 13.5 days in Figure 4. Then, the mass accretion to the WD resumes 20.5 days after it reached the level of full, i.e., t_{vis} delay time. It takes more 6 days that the WD envelope expands to blow a wind again. The total duration of the low state amounts to $13.5 + 20.5 + 6 = 40$ days. Thus, the system repeats the cycle mentioned above.

The modeled system reaches a limit cycle after one cycle of high and low states. The long-term light curve modulations are well reproduced. The time-averaged mass transfer rate is $1.1 \times 10^{-6} M_{\odot} \text{ yr}^{-1}$ and 35% of the transferred matter is blown in the wind, so that the MS loses its mass at the average rate of $3.9 \times 10^{-6} M_{\odot} \text{ yr}^{-1}$ by stripping effects. These values satisfy the conditions of $\dot{M}_{\text{MS}} = \dot{M}_{\text{acc}} + \dot{M}_{\text{strip}}$ and $\dot{M}_{\text{strip}} = 10 \dot{M}_{\text{wind}}$ in averaged values.

It should be noted that our t_{vis} adopted here is 20.5 days, which is tuned to reproduce the duration of optical low states, i.e., $t_{\text{LS}} = 40$ days, because the exact number of t_{vis} is still theoretically not known to us. The duration of low states shortens to $t_{\text{LS}} = 25$ days when $t_{\text{vis}} = 18$ days. Optical low states disappear for $t_{\text{vis}} \lesssim 14$ days. On the other hand, it becomes longer $t_{\text{LS}} = 50$ days when $t_{\text{vis}} = 23$ days. We summarize these results in Table 1. The effect of t_{vis} on the long-term light curves will be discussed more below in relation to other system parameters.

Thus, we are able to reproduce the basic observational features (1)–(4) of RX J0513 summarized in §1. Furthermore, our model naturally explains two other observational features: (5) the WD photosphere continues to expand during the rapid mass accretion phase and still goes on until ~ 20 days after the wind started. This makes a bump of ~ 0.1 mag at the head of optical high states. (6) The WD photosphere gradually shrinks after the rapid mass accretion stops. This also make a gradual decay of ~ 0.2 mag until the end of the wind phase (until the end of the optical high state).

4.2. Mass transfer rate of MS

The mass transfer rate of the MS companion depends on its evolutionary stage and binary parameters (e.g., Li & van den Heuvel 1997; Langer et al. 2000). Since we do not know the exact number of the mass transfer rate in RX J0513, we have examined various values of the original mass transfer rate \dot{M}_{MS} , i.e., 0.6, 0.7, 0.8, 0.9, 1.0, 2.0, 3.0, 5.0 (the template), 7.0, 9.0, 10.0, 15.0, and 20.0 in units of $10^{-6} M_{\odot} \text{ yr}^{-1}$, as summarized in Table 1. The duration of optical high states becomes longer for the higher mass transfer rates of \dot{M}_{MS} . On the other hand, high/low states almost become a 50% duty cycle as the mass transfer rate approaches the critical value, i.e., $\dot{M}_{\text{MS}} \rightarrow \dot{M}_{\text{cr}}$. Some of the calculated light curves are shown in Figure 5.

A remarkable result is that the durations of low states

are kept to be ~ 40 days for a wide range of the mass transfer rates, i.e., $7 \times 10^{-7} M_{\odot} \text{ yr}^{-1} \lesssim \dot{M}_{\text{MS}} \lesssim 6 \times 10^{-6} M_{\odot} \text{ yr}^{-1}$. The duration of high states varies largely from 40 days to 120 days for the same range of the mass transfer rates. This is just the result that we want to explain theoretically, because it is an observational feature as shown in Figure 4 (top panel). The low state gradually shortens and eventually disappears as the mass transfer rate increases to $\dot{M}_{\text{MS}} \gtrsim 1.5 \times 10^{-5} M_{\odot} \text{ yr}^{-1}$ for a set of $t_{\text{vis}} = 20.5$ days and $c_1 = 10.0$. The luminosity of high states is brighter for higher mass transfer rates of \dot{M}_{MS} .

4.3. White dwarf mass

We have also examined various WD masses, i.e., $M_{\text{WD}} = 1.35, 1.2$, and $1.1 M_{\odot}$, with the mass ratio being kept $q = M_{\text{MS}}/M_{\text{WD}} = 2$. The results are shown in Figures 6–8. In general, more massive white dwarfs have a larger wind mass loss rate, so that the duration of the wind phase becomes much shorter. Because we do not know the exact number of t_{vis} , our guided principle is that we tune t_{vis} to satisfy the duration of the low state is 40 days, i.e., $t_{\text{LS}} = 40$ days. For the case of $M_{\text{WD}} = 1.35 M_{\odot}$ shown in Figure 6, we have tuned the viscous timescale t_{vis} at the mass transfer rate of $\dot{M}_{\text{MS}} = 5 \times 10^{-6} M_{\odot} \text{ yr}^{-1}$. The tuned viscous timescale is $t_{\text{vis}} = 15.0$ days. The durations of high/low states are similar to those for $M_{\text{WD}} = 1.3 M_{\odot}$ in Figure 5 except for the relatively short durations. The WD mass in RX J0513 may be less massive than $1.35 M_{\odot}$, because the gradual decay of the light curve in high states seems to be too fast to be compatible with the observation.

For the case of $M_{\text{WD}} = 1.2 M_{\odot}$ shown in Figure 7, we have tuned the viscous timescale at the mass transfer rate of $\dot{M}_{\text{MS}} = 3 \times 10^{-6} M_{\odot} \text{ yr}^{-1}$, i.e., $t_{\text{vis}} = 32.0$ days. The durations of high states are longer than those for $M_{\text{WD}} = 1.3 M_{\odot}$ in Figure 5. The WD mass in RX J0513 may be somewhere between $1.2 M_{\odot}$ and $1.3 M_{\odot}$, because the decay of the light curve in high states seems to be slightly slower than, but in reasonable agreement with, the observation.

For the case of $M_{\text{WD}} = 1.1 M_{\odot}$ shown in Figure 8, we have tuned the viscous timescale at the mass transfer rate of $\dot{M}_{\text{MS}} = 2 \times 10^{-6} M_{\odot} \text{ yr}^{-1}$, i.e., $t_{\text{vis}} = 45.0$ days. The durations of high states are much longer than those for $M_{\text{WD}} = 1.3 M_{\odot}$ in Figure 5. The WD mass of $1.1 M_{\odot}$ may not be the case, because the decay of the light curve in high states is too slow to be compatible with the observation.

4.4. Mass stripping effect

It is a difficult work to accurately estimate the effect of mass-stripping, that is, to determine the coefficient of c_1 in equation (12). Therefore, we calculate two other cases of c_1 , i.e., $c_1 = 5$ and $c_1 = 1.5$ and examine how the light curves depend on the coefficient. It is obvious that strong modulation of the mass transfer rate never occurs for the case of $c_1 \leq 1$ because there is no case of $\dot{M}_{\text{MS}} < \dot{M}_{\text{strip}} = c_1 \dot{M}_{\text{wind}} (\leq \dot{M}_{\text{wind}} < \dot{M}_{\text{acc}} < \dot{M}_{\text{MS}})$. Our calculated models and their parameters are listed in Table 1.

For the case of $c_1 = 5$ shown in Figure 9, the overall features of light curves are essentially similar to the case of $c_1 = 10$ shown in Figure 5. Main differences are

that (1) the tuned viscous timescale is $t_{\text{vis}} = 36.0$ days at $\dot{M}_{\text{MS}} = 2 \times 10^{-6} M_{\odot} \text{ yr}^{-1}$, much longer than $t_{\text{vis}} = 20.5$ days for $c_1 = 10$, and (2) bumps at the head of high states continue for a much longer period and may not be compatible with the observation.

For the case of $c_1 = 1.5$ shown in Figure 10, a new thing is the appearance of no modulation in mass transfer for a range of $0.67 \times 10^{-6} M_{\odot} \text{ yr}^{-1} < \dot{M}_{\text{MS}} < 1.5 \times 10^{-6} M_{\odot} \text{ yr}^{-1}$. The tuned viscous timescale is $t_{\text{vis}} = 62.0$ days at $\dot{M}_{\text{MS}} = 2 \times 10^{-6} M_{\odot} \text{ yr}^{-1}$. Bumps at the head of high states continue for about 40 days. Both the viscous timescale and the duration of bumps are much longer than those for $c_1 = 10$ and $c_1 = 5$. The long duration of bumps is not compatible with the observation.

An important result in this subsection is that modulation in mass transfer occurs and optical high/low states appear even for relatively low efficiencies of mass-stripping on the MS, i.e., for $c_1 = 1.5$, if the viscous timescale is relatively long, i.e., $t_{\text{vis}} = 62$ days. Such a low case of c_1 may correspond to a low velocity case of winds as understood from equation (14) and a relatively long viscous timescale is realized for binaries with a longer orbital period, for example, longer than a day, as derived from equation (17).

5. DISCUSSION

It has been argued that only a viable mechanism for the transition between the optical high/X-ray off and optical low/X-ray on states is the contraction/expansion of the WD photosphere resulting from the variation of the mass accretion rate to the WD (e.g., Meyer-Hofmeister et al. 1997; Pakull et al. 1993; Reinsch et al. 1996, 2000; Southwell et al. 1996), although a few other mechanisms have ever been proposed (see, e.g., discussion of Southwell et al. 1996). Therefore, we first examine whether or not this mechanism can explain all the observational features.

Reinsch et al. (2000) detected a very sharp rise (< 3 days) and a steep decline (< 2 days) in supersoft X-rays by a factor of > 100 . This requires a contraction/expansion of the WD photosphere by a factor of > 7 and an increase/decrease of the photospheric temperature by a factor of > 3 (Reinsch et al. 2000). We have estimated the timescale of contracting/expanding WD envelopes based on our wind and static solutions. The WD photosphere gradually shrinks during the wind phase while it begins to contract most rapidly just after the wind stops (see the bottom panel of Fig. 4). Even for this most rapid shrink phase, it takes about three Kelvin-Helmholtz timescale to shrink by a factor of four, i.e.,

$$t_{\text{contract}} \sim 3\tau_{\text{KH}}, \quad (21)$$

from our model calculations. This Kelvin-Helmholtz timescale is defined by

$$\tau_{\text{KH}} = \frac{\Delta E_{\text{env, thermal}}}{L}, \quad (22)$$

where $\Delta E_{\text{env, thermal}}$ is the thermal energy of the WD envelope, and L the luminosity of the WD, just when the wind stops. These contraction timescales just after the wind stops are plotted against various WD masses in Figure 11. It is obvious that the rapid (< 2 days) change in the soft X-ray flux cannot be explained by the contraction of the WD photosphere even if we assume the extreme case of $M_{\text{WD}} = 1.377 M_{\odot}$ (at least, for $Z = 0.004$).

For the expansion case of the WD photosphere during the rapid mass accretion phase, our steady-state wind model does not correctly include the compression term by accretion so that the estimated timescale is not so accurate. In this sense, our numerical results cannot give a strong constraint on the timescale of photospheric expansion. It should be pointed out, however, that usual time-dependent Henyey methods fail to be converged in a rapidly expanding photosphere of WDs and are now unable to involve wind mass loss.

Reinsch et al. (2000) suggested a characteristic decay timescale of 34 days from the exponential decay of supersoft X-rays in an optical low state. In our model, there are two possibilities. One is the timescale of expansion/contraction of the WD photosphere and the other is the viscous timescale of the accretion disk, t_{vis} . If this 34 days timescale is related to the expansion/contraction timescale of a WD envelope, its WD mass is somewhere between $1.2 M_{\odot}$ and $1.3 M_{\odot}$ for the metallicity of $Z = 0.004$ as shown in Figure 11. This mass range of the WD is consistent with our long-term light curve modulations. On the other hand, if it indicates that $t_{\text{vis}} = 34$ days, the ranges of the parameters are also suggested to be $M_{\text{WD}} = 1.2 - 1.3 M_{\odot}$ and $c_1 = 5 - 10$ from Table 1. These are also consistent with our long-term light curve modulations.

Southwell et al. (1996) suggested that star spots on the secondary surface cover the L1 point, resulting in a decreased mass transfer rate from the secondary. This mechanism has been originally suggested by Livio & Pringle (1994) for the VY Scl stars. In RX J0513, however, it is very unlikely that the MS companion develops star spots on its surface, because its mass is suggested to be $2-3 M_{\odot}$, not having a deep surface convection.

Very recently, Hutchings et al. (2002) reported radial velocity modulations of $\sim 117 \pm 40$ and $54 \pm 10 \text{ km s}^{-1}$ for the broad O VI emission and Lyman absorption, respectively. If these trace the motions of the hot and cool components, respectively, the estimated mass ratio is $q = M_{\text{MS}}/M_{\text{WD}} = 2.2 \pm 1.2$, being consistent with our assumption of $q = 2$. The corresponding inclination angle is $i = 28^{\circ} \pm 10^{\circ}$ for our case of $M_{\text{WD}} = 1.3 M_{\odot}$ and $M_{\text{MS}} = 2.6 M_{\odot}$, which is a bit larger than our assumption of $i = 10^{\circ}$. Then, we have examined how the long-term light curve depends on the inclination. Additional four cases of the inclination angle, i.e., $i = 0^{\circ}, 20^{\circ}, 28^{\circ}$, and 35° , are calculated. The results are also shown in Figure 12, which are not so much different in shape from the case of $i = 10^{\circ}$, but the brightness in optical high states decreases by a factor of $\cos i$.

Cowley et al. (2002) have reanalyzed the MACHO data for eight years and determined a new orbital period and a new ephemeris. They found that the orbital modulations of the optical light curve are different in shape between the optical high and low states. The orbital modulation dip is much broader in the high state than in the low state. Assuming an inclination angle of $i = 28^{\circ}$, we have calculated two orbital modulations each for the optical high state and for the optical low state as shown in Figure 13. The observational broad and shallow orbital modulations in the optical high state are reasonably reproduced as well as their full extents (amplitudes) of $\Delta V \sim 0.06 \text{ mag}$. On

the other hand, the full extents of the orbital modulations become larger (deeper) to $\Delta V \sim 0.09 \text{ mag}$ in the optical low state, being consistent with the observation.

6. CONCLUSIONS

A new self-sustained model for the long-term light curve variations of RX J0513.9–6951 is formulated based on our optically thick wind model of mass-accreting white dwarfs. We also show that RX J0513.9–6951 is the first beautiful example of the accretion wind evolution, which is a key evolutionary process to Type Ia supernovae (e.g., Hachisu 2002; Hachisu & Kato 2001).

We have already shown that, when the mass accretion rate to a WD exceeds the critical rate $\dot{M}_{\text{cr}} \approx 0.75 \times 10^{-6} (M_{\text{WD}}/M_{\odot} - 0.4) M_{\odot} \text{ yr}^{-1}$, optically thick strong winds begin to blow from the WD. As a result, a formation of common envelope is avoided. In such a situation, the WD accretes and burns hydrogen atop the WD at the critical rate. The excess matter transferred to the WD above the critical rate is expelled by winds (Hachisu et al. 1996, 1999a,b). This is called the accretion wind evolution (Hachisu & Kato 2001). Unfortunately, no such systems have ever been discovered. Here, we report that the LMC supersoft X-ray source RX J0513.9–6951 is the first example of such an object, i.e., just in the accretion wind evolution.

We summarize our main results as follows:

1. Mass ejection in the accretion wind evolution does occur not continuously but intermittently because the mass transfer is attenuated by strong winds. The strong winds collide with the secondary and strip off the very surface layer of the secondary. Properly formulating this mass stripping effect and the ensuing decay of mass transfer rate, we obtain, in a self-sustained manner, on/off of mass transfer from the companion star.
2. A light curve modeling on the 2000 outburst of the recurrent nova CI Aql showed that the size of the disk around the white dwarf extends widely up to the companion star or over only during the strong wind phase (Hachisu & Kato 2003). Including this large extension of a disk in a strong wind phase, we are able to reproduce the transition between the optical high and low states of the LMC supersoft X-ray source RX J0513.9–6951: When a strong wind occurs, the very surface layer of the disk is blown in the wind and the disk expands up to the companion or over. This large extension of the irradiation area makes a sharp $\sim 1 \text{ mag}$ rise in the optical light curve. On the other hand, it drops sharply by a magnitude when the wind stops because the size of the disk returns to its original size.
3. In optically thick winds, the mass loss rate rises to $\dot{M}_{\text{wind}} \gtrsim 1 \times 10^{-8} M_{\odot} \text{ yr}^{-1}$ one day after the wind starts. This can obscure completely soft X-rays. On the other hand, the wind mass loss rate drops from $\dot{M}_{\text{wind}} \sim 1 \times 10^{-8} M_{\odot} \text{ yr}^{-1}$ to zero in within a day, which enables a short ($< 1 \text{ day}$) timescale of soft X-ray emergence. Thus, we are also able to reproduce a very rapid emergence/decay of supersoft X-rays in within a day or so.
4. We abstract two important system parameters. One is the viscous timescale of the accretion disk, t_{vis} , and the other is the efficiency of mass-stripping by winds, c_1 , defined by $\dot{M}_{\text{strip}} = c_1 \dot{M}_{\text{wind}}$. Both of them should be determined self-consistently but are not accurately deter-

mined at least at the present time like the α -parameter of Shakura & Sunyaev (1973). We are able to reproduce the optical high/low states for reasonable ranges of the system parameters, i.e., 20 days $\lesssim t_{\text{vis}} \lesssim 60$ days and $1.5 \lesssim c_1 \lesssim 10$.

5. The original mass transfer rate from the main-sequence companion is probably constant in time. Even if this original mass transfer rate varies from several times $10^{-7} M_{\odot} \text{ yr}^{-1}$ to several times $10^{-6} M_{\odot} \text{ yr}^{-1}$, by a factor of ten, the duration of optical low states hardly changes, i.e., stays around ~ 40 days, for a fixed set of (t_{vis}, c_1) . On the other hand, the duration of optical high states varies from ~ 40 days to ~ 120 days for the same range of the original mass transfer rate. These durations of optical high/low states are the prominent features of the MACHO observations (Alcock et al. 1996; Cowley et al. 2002).

6. The white dwarf photosphere expands and blows a wind during the rapid mass accretion phase. The photospheric expansion still goes on for a while after the wind suppresses the mass transfer, because the accretion disk supplies mass to the WD for a draining time (viscous timescale). This makes a bump of ~ 0.1 mag at the head of the optical high state. The duration of this bump may determine the value of t_{vis} . The WD photosphere gradually shrinks after the rapid mass accretion stops. This makes a gradual decay of ~ 0.2 mag in the optical light curve until the end of the wind phase (until the end of the optical high state). These two light curve features clearly appear in the MACHO observation (Alcock et al. 1996).

7. Comparison of the modeled light curves with the observation implies that the mass of the white dwarf is about $1.2 - 1.3 M_{\odot}$, the original mass transfer rate $(2 - 3) \times 10^{-6} M_{\odot} \text{ yr}^{-1}$, the viscous timescale 20–40 days, and the efficiency of stripping by winds $c_1 = 5 - 10$.

8. The on/off timescales of supersoft X-rays are as short as one or two days (Reinsch et al. 2000). Only the contraction/expansion of the white dwarf photosphere cannot explain the rapid emergence/decay of supersoft X-rays because the contraction/expansion timescales of the white dwarf photosphere are too long to reproduce such a rapid emergence/decay of supersoft X-rays.

The white dwarf in RX J0513.9–6951 is now constantly growing in mass at the critical rate of \dot{M}_{cr} . We expect that the mass of the white dwarf increases up to near the Chandrasekhar mass and the white dwarf eventually explodes as a Type Ia supernova. Thus, RX J0513.9–6951 is the first beautiful example of the accretion wind evolution, which is a key evolutionary process in a recently developed evolutionary path to Type Ia supernovae (e.g., Hachisu et al. 1996, 1999a,b; Hachisu & Kato 2001; Langer et al. 2000; Li & van den Heuvel 1997).

We are indebted to F. Meyer and Emi Meyer-Hofmeister for stimulating us to work on RX J0513.9–6951 during our stay at the Max-Planck Institute for Astrophysics. This research has been supported in part by a Grant-in-Aid for Scientific Research (11640226) from the Japan Society for the Promotion of Science.

REFERENCES

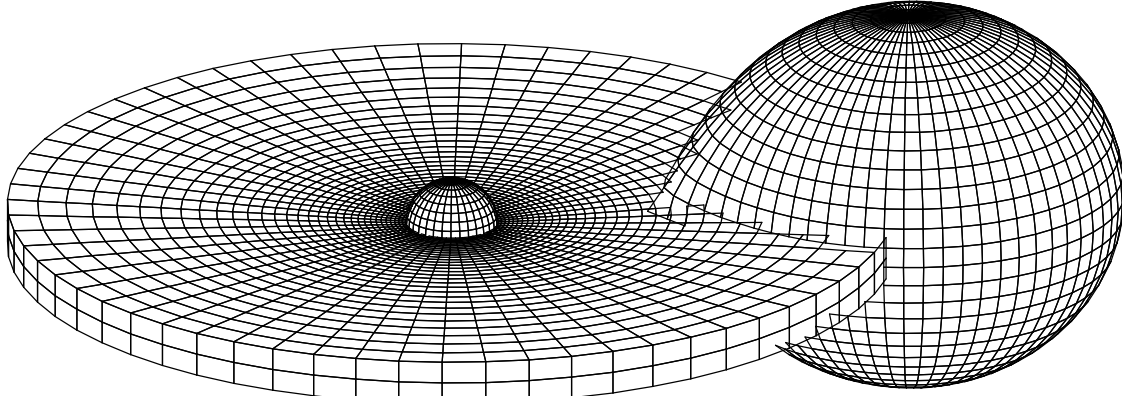
- Alcock, C. et al. 1996, MNRAS, 280, L49
 Cowley, A.P., Schmidtke, P.C., Crampton, D., & Hutchings, J.B. 2002, AJ, 124, 2233
 Crampton, D., Hutchings, J. B., Cowley, A. P., Schmidtke, P. C., McGrath, T. K., O'Donoghue, D., & Harrop-Allin, M. K. 1996, ApJ, 456, 320
 Fagotto, F., Bressan A., Bertelli G., Chiosi C. 1994, A&AS, 105, 29
 Gänsicke, B. T., van Teeseling, A., Beuermann, K., & de Martino, D. 1998, A&A, 333, 163
 Hachisu, I. 2002, The Physics of Cataclysmic Variables and Related Objects, ASP Conference Proceedings, 261, Eds. B. T. Gänsicke, K. Beuermann, & K. Reinsch (San Francisco: Astronomical Society of the Pacific), p. 605
 Hachisu, I., & Kato, M. 2001, ApJ, 558, 323
 Hachisu, I., & Kato, M. 2003, ApJ, in press (astro-ph/0301489)
 Hachisu, I., Kato, M., & Nomoto, K. 1996, ApJ, 470, L97
 Hachisu, I., Kato, M., & Nomoto, K. 1999a, ApJ, 522, 487
 Hachisu, I., Kato, M., Nomoto, K., & Umeda, H. 1999b, ApJ, 519, 314
 Hutchings, J. B., Winter, K., Cowley, A. P., Schmidtke, P. C., & Crampton, D. 2002, AJ, 124, 2833
 Iben, I. Jr., & Tutukov, A. V. 1984, ApJS, 54, 335
 Kato, M., & Hachisu, I., 1994, ApJ, 437, 802
 Langer, N., Deutschmann, A., Wellstein, S., & Höflich, P. 2000, A&A, 362, 1046
 Li, X.-D., & van den Heuvel, E. P. J. 1997, A&A, 322, L9
 Livio, M., & Pringle, J. E. 1994, ApJ, 427, 956
 Meyer-Hofmeister, E., Schandl, S., Meyer, F. 1997, A&A, 321, 245
 Pakull, M. W., Moch, C., Bianchi, L., Thomas, H.-C., Guibert, J., Beaulieu, J. P., Grison, P., & Schaeidt, S. 1993, A&A, 278, L39
 Reinsch, K., van Teeseling, A., Beuermann, K., & Abbott, T. M. C. 1996, A&A, 309, L11
 Reinsch, K., van Teeseling, A., King, A. R., & Beuermann, K. 2000, A&A, 354, L37
 Shakura, N. I., & Sunyaev, R. A. 1973, A&A, 24, 337
 Schaeidt, S., Hasinger, G., & Truemper, J. 1993, A&A, 270, L9
 Schandl, S., Meyer-Hofmeister, E., & Meyer, F. 1997, A&A, 318, 73
 Southwell, K. A., Livio, M., Charles, P. A., O'Donoghue, D., & Sutherland, W. J. 1996, ApJ, 470, 1065
 van den Heuvel, E. P. J., Bhattacharya, D., Nomoto, K., & Rappaport, S. 1992, A&A, 262, 97
 Webbink, R. F. 1984, ApJ, 277, 355

TABLE 1
DURATIONS OF HIGH AND LOW STATES

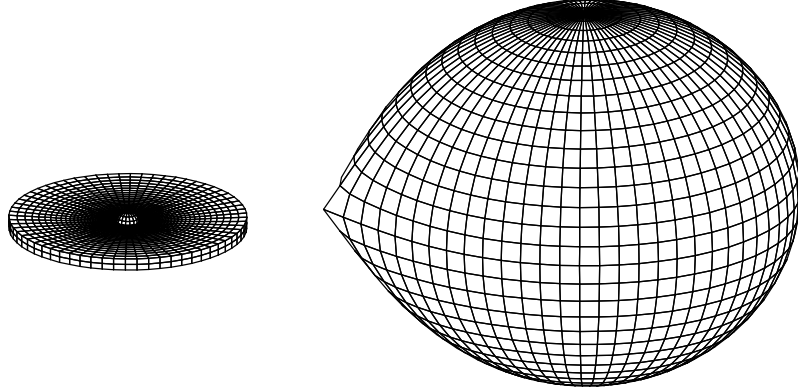
M_{WD} (M_{\odot})	\dot{M}_{MS} ($10^{-6} M_{\odot} \text{ yr}^{-1}$)	t_{vis} (day)	c_1	high (days)	low (days)	light curve	comments
1.35	1.0	15.0	10.0	30	30	Fig.6a	
1.35	2.0	15.0	10.0	40	40	Fig.6b	
1.35	5.0	15.0	10.0	70	40	Fig.6c	fix t_{vis}
1.35	10.	15.0	10.0	90	35	Fig.6d	
1.35	5.0	20.5	10.0	80	70		
1.3	0.6	20.5	10.0	0	∞		no winds
1.3	0.7	20.5	10.0	40	45		
1.3	0.8	20.5	10.0	40	45		
1.3	0.9	20.5	10.0	40	45	Fig.5a	
1.3	1.0	20.5	10.0	45	35	Fig.5b	
1.3	2.0	20.5	10.0	65	40	Fig.5c	
1.3	3.0	20.5	10.0	85	40	Fig.5d	
1.3	5.0	20.5	10.0	110	40	Fig.4b	fix t_{vis}
1.3	7.0	20.5	10.0	130	30	Fig.5e	
1.3	9.0	20.5	10.0	140	25		
1.3	10.	20.5	10.0	150	20	Fig.5f	
1.3	15.	20.5	10.0	160	2	Fig.5g	
1.3	20.	20.5	10.0	∞	0	Fig.5h	modulation ^a
1.3	5.0	14.0	10.0	∞	0		modulation
1.3	5.0	16.0	10.0	95	15		
1.3	5.0	18.0	10.0	100	25		
1.3	5.0	23.0	10.0	115	50		
1.3	0.7	36.0	5.0	75	50	Fig.9a	
1.3	1.0	36.0	5.0	85	40	Fig.9b	
1.3	2.0	36.0	5.0	105	40	Fig.9c	fix t_{vis}
1.3	3.0	36.0	5.0	120	30	Fig.9e	
1.3	5.0	20.5	5.0	∞	0		modulation
1.3	5.0	35.0	5.0	∞	0		modulation
1.3	5.0	45.0	5.0	165	40		
1.3	5.0	50.0	5.0	175	60		
1.3	2.0	45.0	5.0	115	65		
1.3	2.0	40.0	5.0	110	50		
1.3	2.0	34.0	5.0	100	35		
1.3	2.0	33.0	5.0	95	30		
1.3	2.0	30.0	5.0	90	25		
1.3	1.0	62.0	1.5	∞	0	Fig.10a	no modulation ^b
1.3	2.0	62.0	1.5	110	40	Fig.10c	fix t_{vis}
1.3	3.0	62.0	1.5	115	35	Fig.10d	
1.3	5.0	62.0	1.5	195	25	Fig.10e	
1.3	1.0	36.0	1.5	∞	0		no modulation
1.3	2.0	36.0	1.5	∞	0		modulation
1.3	5.0	36.0	1.5	∞	0		modulation
1.3	2.0	60.0	1.5	150	35		
1.3	5.0	60.0	1.5	190	25		
1.2	1.0	32.0	10.0	80	45	Fig.7a	
1.2	2.0	32.0	10.0	120	45	Fig.7b	
1.2	3.0	32.0	10.0	155	40	Fig.7d	fix t_{vis}
1.2	5.0	32.0	10.0	200	30	Fig.7e	
1.2	3.0	35.0	10.0	160	50		
1.2	5.0	35.0	10.0	210	40		
1.2	3.0	33.5	10.0	160	50		
1.2	3.0	35.0	10.0	160	50		
1.2	5.0	35.0	10.0	210	40		
1.2	5.0	20.5	10.0	∞	0		modulation
1.2	5.0	30.0	10.0	195	15		
1.2	5.0	40.0	10.0	225	70		
1.1	0.6	45.0	10.0	115	55	Fig.8a	
1.1	1.0	45.0	10.0	120	50	Fig.8b	
1.1	2.0	45.0	10.0	195	40	Fig.8d	fix t_{vis}
1.1	3.0	45.0	10.0	250	20	Fig.8e	
1.1	2.0	40.0	10.0	175	25		
1.1	2.0	50.0	10.0	205	65		
1.1	5.0	20.5	10.0	∞	0		modulation
1.1	5.0	40.0	10.0	∞	0		modulation
1.1	5.0	60.0	10.0	380	70		

^a mass accretion rate \dot{M}_{acc} is modulated by winds

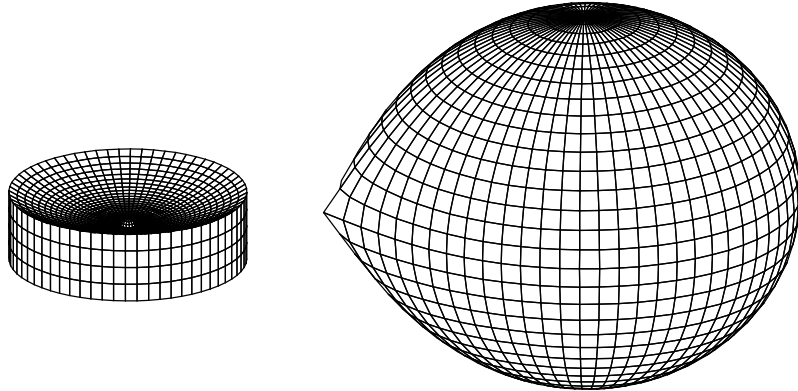
^b mass accretion rate is not modulated by winds but constant in time



(a) optically thick wind phase



(b) just after the wind stops



(c) mass accretion makes a spray

FIG. 1.— Configurations of our modeled RX J0513.9–6951 are illustrated: (a) in the massive wind phase (X-ray off), (b) just after the wind stops (X-ray on), and (c) during a rapid mass accretion phase soon after the wind stops (X-ray on). The cool component (*right*) is a slightly evolved main-sequence (MS) companion ($2.6M_{\odot}$) filling its inner critical Roche lobe. The north and south polar areas of the cool component are irradiated by the hot component ($1.3 M_{\odot}$ white dwarf, *left*). The separation is $a = 5.53R_{\odot}$; the effective radii of the inner critical Roche lobes are $R_1^* = 1.77R_{\odot}$, and $R_2^* = R_2 = 2.43R_{\odot}$, for the primary WD and the secondary MS companion, respectively. (a) The surface of the accretion disk is blown in the wind and its optically thick outer edge extends up to the companion star or over. The large velocity difference between the wind and the disk surface certainly drives the Kelvin-Helmholtz instability at the interface, so that the very surface layer of the disk is dragged away as an almost free stream going outward. This surface free stream is initially optically thick but becomes optically thin outside because of geometrical dilution effect. We regard the transition from optically thick to thin as the edge of the disk. (b) The disk shrinks to a normal size ($0.7 - 0.8$ times the Roche lobe radius) in several dynamical timescales, i.e., several orbital periods after the wind stops. (c) A rapid mass accretion makes a spray around the disk edge.

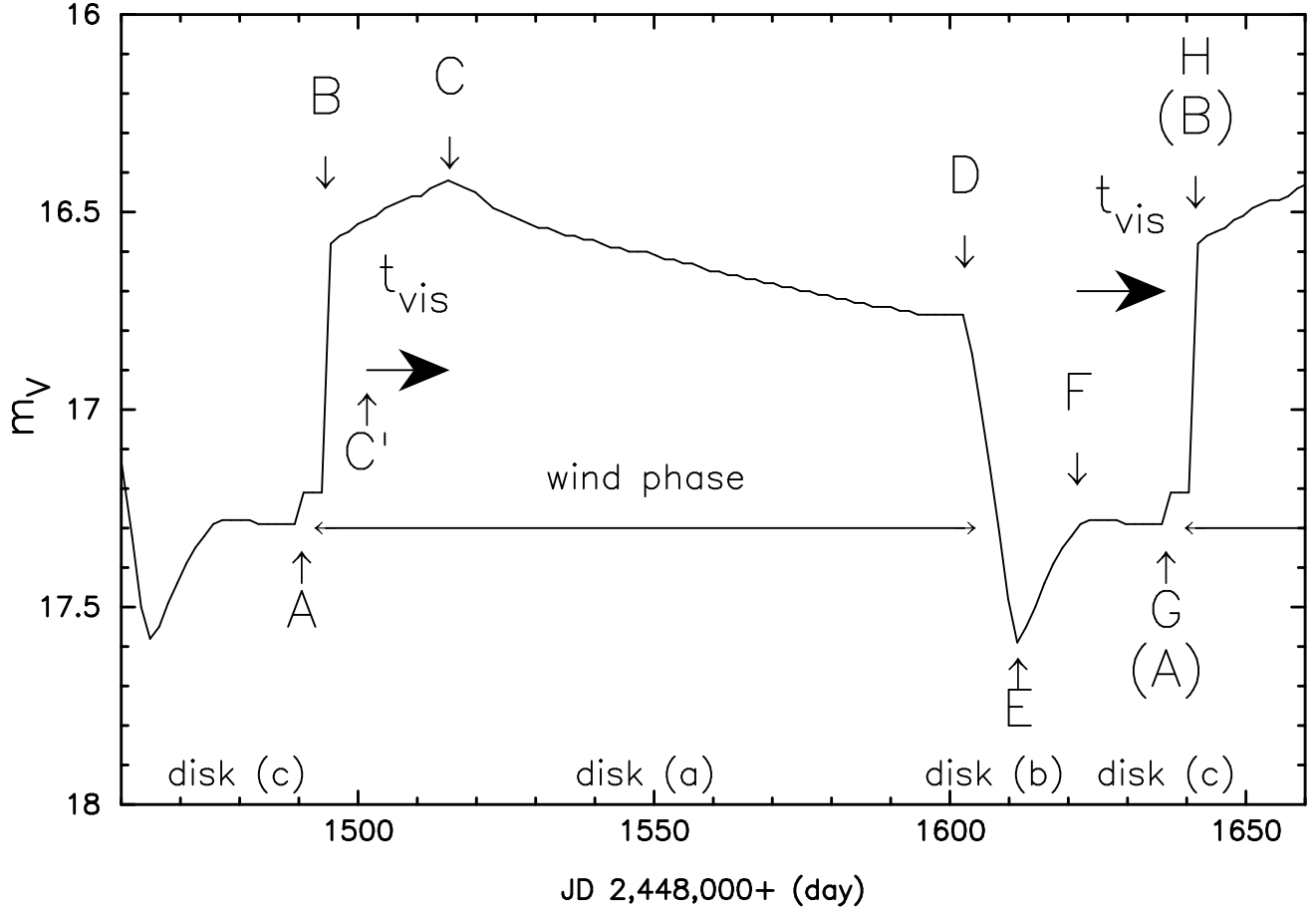


FIG. 2.— A modeled light curve for a limit cycle is plotted. A rapid mass accretion to the WD begins at A. The envelope of the WD expands to blow an optically thick wind at B. The strong wind causes a quick rise of the optical light curve, because the disk expands to a few to several times the previous size (see disk configuration (a) in Fig. 1). The massive wind certainly absorb supersoft X-rays. Thus, this is the optical high/X-ray off state. Because the wind hits and then strips-off the very surface layer of the MS companion, mass transfer from the MS is heavily suppressed and stops at C'. However, the mass accretion to the WD still continues during a viscous timescale of the accretion disk, i.e., t_{vis} . After a large part of the mass in the accretion disk is drained, the mass accretion to the WD virtually stops at C. The mass of the WD envelope is now gradually decreasing due mainly to wind mass loss. Then the WD photosphere is also gradually shrinking. This makes a slow decline in the optical light curve. The wind eventually stops at D. The disk shrinks to a normal size at E, causing a sharp drop of the optical light curve (see disk configuration (b) in Fig. 1). The mass transfer from the MS resumes at E, and then the edge of the disk flares up at F (see disk configuration (c) in Fig. 1). It takes several dynamical timescales to change from E to F. We expect copious supersoft X-rays after the wind stops. This is the optical low/X-ray on state. A rapid mass accretion to the WD resumes at G(=A), because it takes a viscous timescale, i.e., t_{vis} , that the matter reaches the WD surface via an accretion disk. This cycle is repeated.

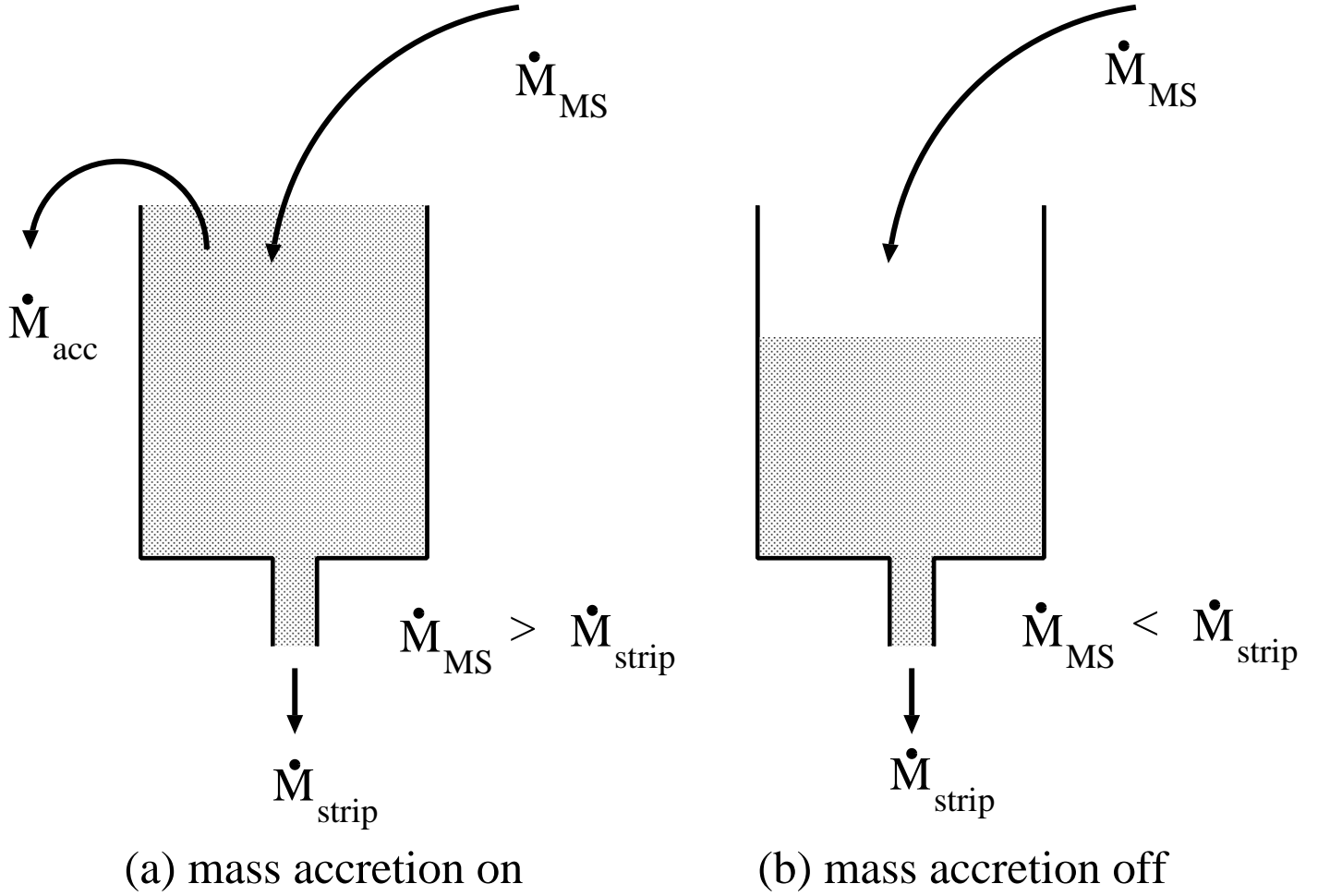


FIG. 3.— Schematic illustrations for the flow from the secondary main-sequence companion: (a) mass transfer is going on when the stripping effect by the wind is smaller than the original mass transfer rate, i.e., $\dot{M}_{\text{strip}} < \dot{M}_{\text{MS}}$. (b) Mass transfer stops if the stripping effect by the wind is larger than the original mass transfer rate, i.e., $\dot{M}_{\text{strip}} \geq \dot{M}_{\text{MS}}$. We are able to know when mass transfer resumes again by checking whether or not $M_{\text{flow}} \geq 0$ by integrating equation (16), where M_{flow} indicates the level of flow ($M_{\text{flow}} = 0$ at full).

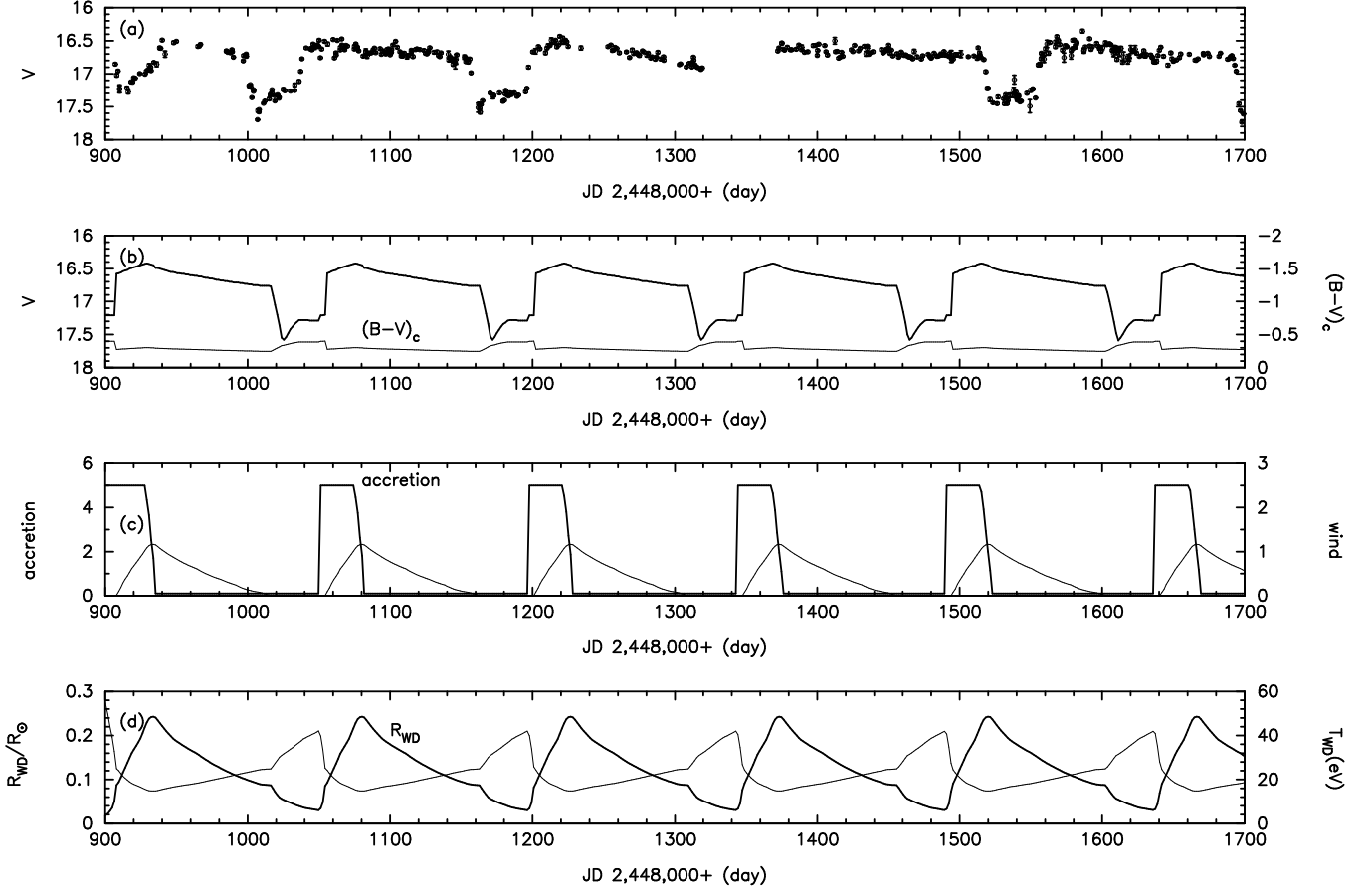


FIG. 4.— Numerical results of our RX J0513.9–6951 models are shown against time (JD 2,448,000+) together with observational light curve: (a) Observational V -magnitudes (taken from Alcock et al. 1996). (b) Calculated V -magnitudes (*thick solid line*) together with $B - V$ color (*thin solid line*). (c) Mass accretion rate to the WD (\dot{M}_{acc} , *thick solid*) and wind mass loss rate from the WD (\dot{M}_{wind} , *thin solid*), both in units of $10^{-6} M_{\odot} \text{yr}^{-1}$. (d) Photospheric radius of the WD envelope in units of R_{\odot} (*thick solid*) and surface temperature of the WD envelope in units of eV (*thin solid*). The model parameters are summarized in Table 1, i.e., $M_{\text{WD}} = 1.3 M_{\odot}$, $\dot{M}_{\text{MS}} = 5.0 \times 10^{-6} M_{\odot} \text{yr}^{-1}$, $c_1 = 10.0$, and $t_{\text{vis}} = 20.5$ days. Direct fitting to the brightness of the observational light curves indicates an apparent distance modulus of $(m - M)_V = 18.7$.

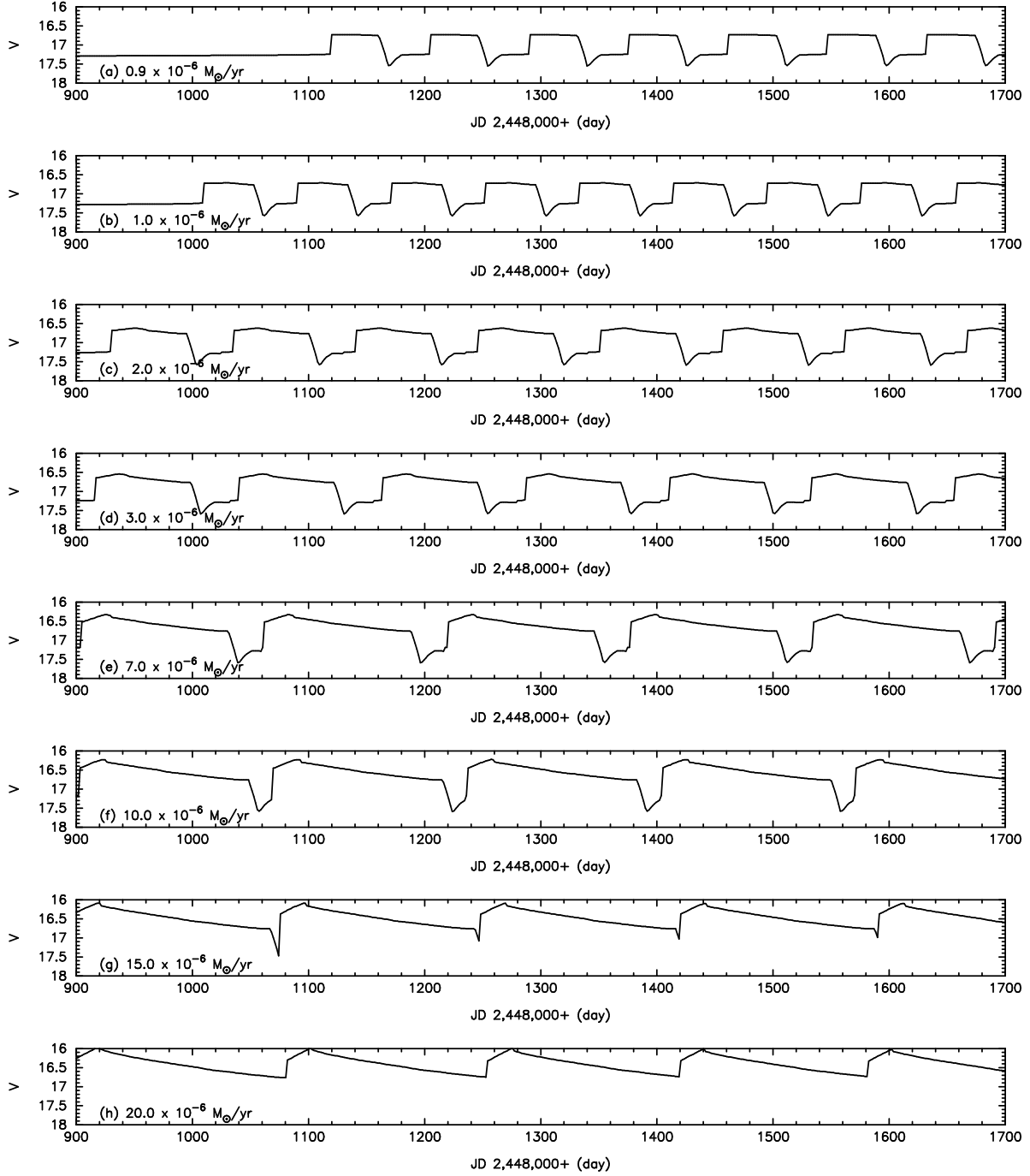


FIG. 5.— Calculated V-magnitude light curves are plotted against time (JD 2,448,000+) for various mass transfer rates. The model parameters for each case are also summarized in Table 1: (a) $\dot{M}_{\text{MS}} = 0.9 \times 10^{-6} M_{\odot} \text{ yr}^{-1}$. It takes about 210 days for this relatively low mass accretion rate that the WD envelope mass reaches $6.5 \times 10^{-7} M_{\odot}$, where the WD begins to blow a wind, from the initial envelope mass of $5.0 \times 10^{-7} M_{\odot}$. The first flat part corresponds to a part of this 210 days. (b) $\dot{M}_{\text{MS}} = 1.0 \times 10^{-6} M_{\odot} \text{ yr}^{-1}$, (c) $\dot{M}_{\text{MS}} = 2.0 \times 10^{-6} M_{\odot} \text{ yr}^{-1}$, (d) $\dot{M}_{\text{MS}} = 3.0 \times 10^{-6} M_{\odot} \text{ yr}^{-1}$, (e) $\dot{M}_{\text{MS}} = 7.0 \times 10^{-6} M_{\odot} \text{ yr}^{-1}$, (f) $\dot{M}_{\text{MS}} = 10. \times 10^{-6} M_{\odot} \text{ yr}^{-1}$, (g) $\dot{M}_{\text{MS}} = 15. \times 10^{-6} M_{\odot} \text{ yr}^{-1}$, (h) $\dot{M}_{\text{MS}} = 20. \times 10^{-6} M_{\odot} \text{ yr}^{-1}$. Each model has $M_{\text{WD}} = 1.3 M_{\odot}$, $c_1 = 10.0$, and $t_{\text{vis}} = 20.5$ days in common. We adopt the apparent distance modulus of $(m - M)_V = 18.7$.

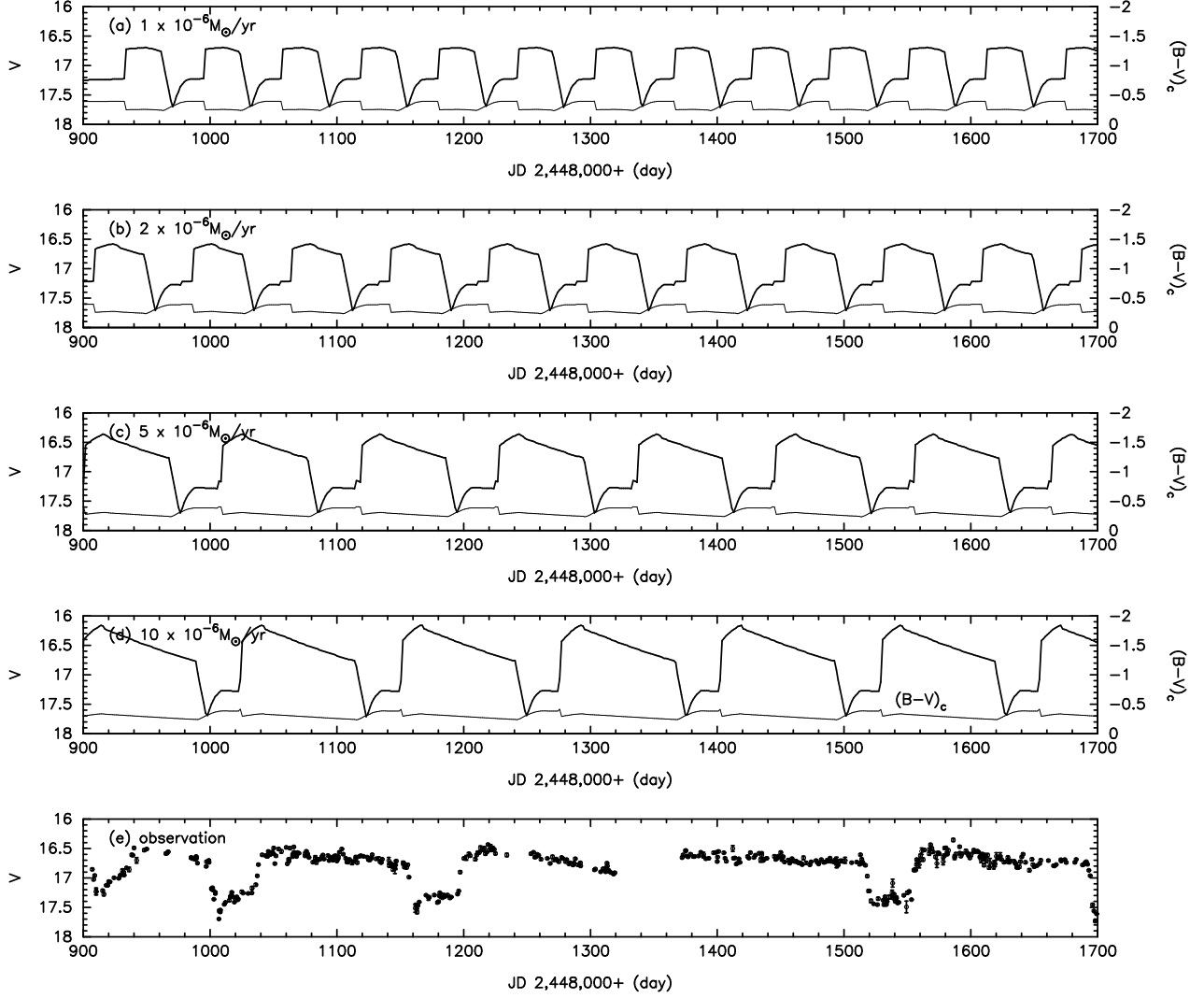


FIG. 6.— Calculated V -magnitude and $B-V$ color light curves are plotted against time (JD 2,448,000+) for our $M_{\text{WD}} = 1.35 M_{\odot}$ models. The model parameters are summarized in Table 1: (a) $\dot{M}_{\text{MS}} = 1.0 \times 10^{-6} M_{\odot} \text{ yr}^{-1}$, (b) $\dot{M}_{\text{MS}} = 2.0 \times 10^{-6} M_{\odot} \text{ yr}^{-1}$, (c) $\dot{M}_{\text{MS}} = 5.0 \times 10^{-6} M_{\odot} \text{ yr}^{-1}$, (d) $\dot{M}_{\text{MS}} = 10.0 \times 10^{-6} M_{\odot} \text{ yr}^{-1}$, and (e) observational V -magnitudes are also added (taken from Alcock et al. 1996). The other parameters of $c_1 = 10.0$ and $t_{\text{vis}} = 15.0$ days are common among the model light curves. We adopt the apparent distance modulus of $(m-M)_V = 18.7$.

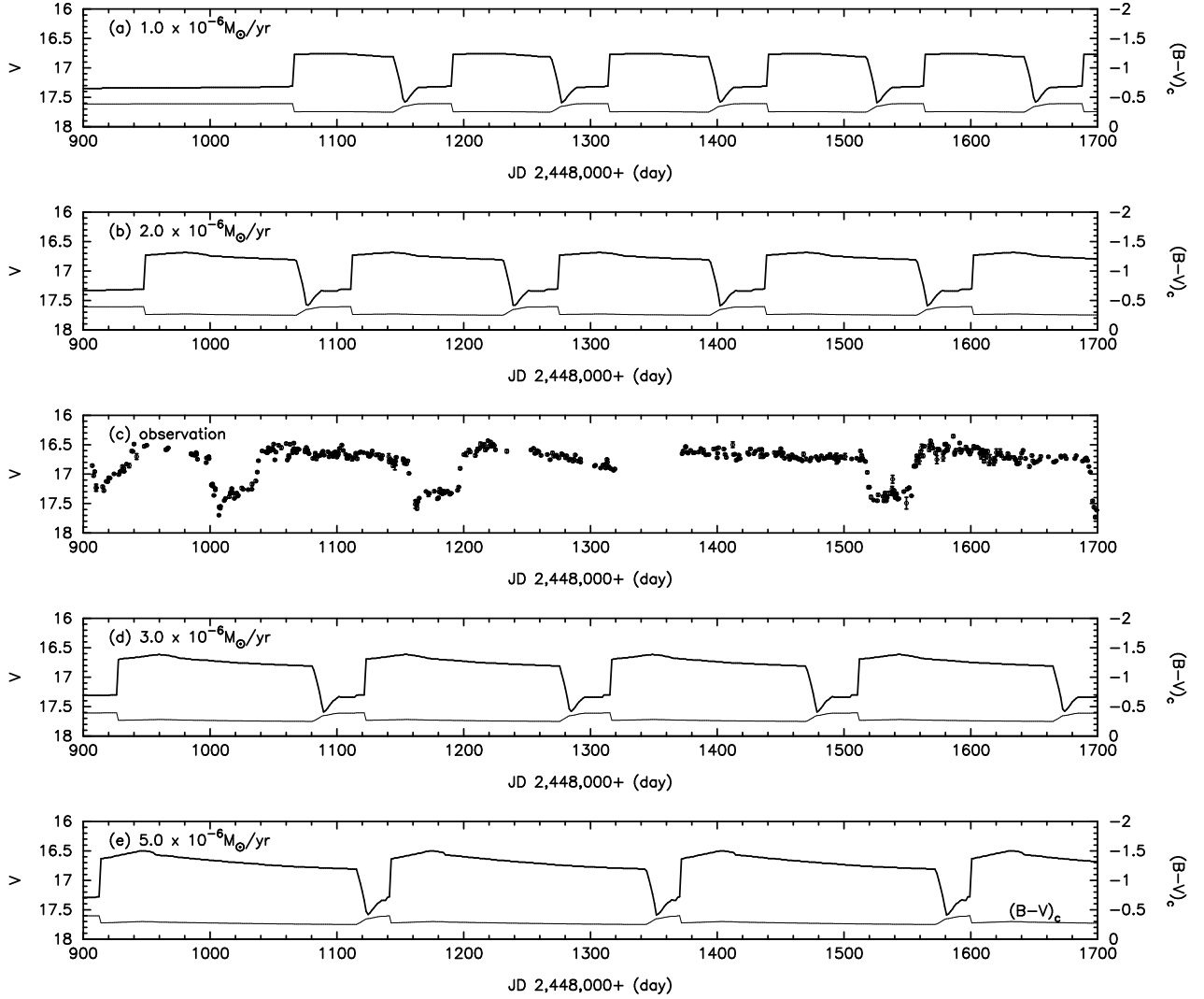


FIG. 7.— Calculated V -magnitude and $B - V$ color light curves are plotted against time (JD 2,448,000+) for our $M_{\text{WD}} = 1.2 M_{\odot}$ models. The model parameters are summarized in Table 1: (a) $\dot{M}_{\text{MS}} = 1.0 \times 10^{-6} M_{\odot} \text{ yr}^{-1}$, (b) $\dot{M}_{\text{MS}} = 2.0 \times 10^{-6} M_{\odot} \text{ yr}^{-1}$, (c) observational V -magnitudes (taken from Alcock et al. 1996), (d) $\dot{M}_{\text{MS}} = 3.0 \times 10^{-6} M_{\odot} \text{ yr}^{-1}$, (e) $\dot{M}_{\text{MS}} = 5.0 \times 10^{-6} M_{\odot} \text{ yr}^{-1}$. The other parameters of $c_1 = 10.0$ and $t_{\text{vis}} = 32.0$ days are common among the model light curves. We adopt the apparent distance modulus of $(m - M)_V = 18.7$.

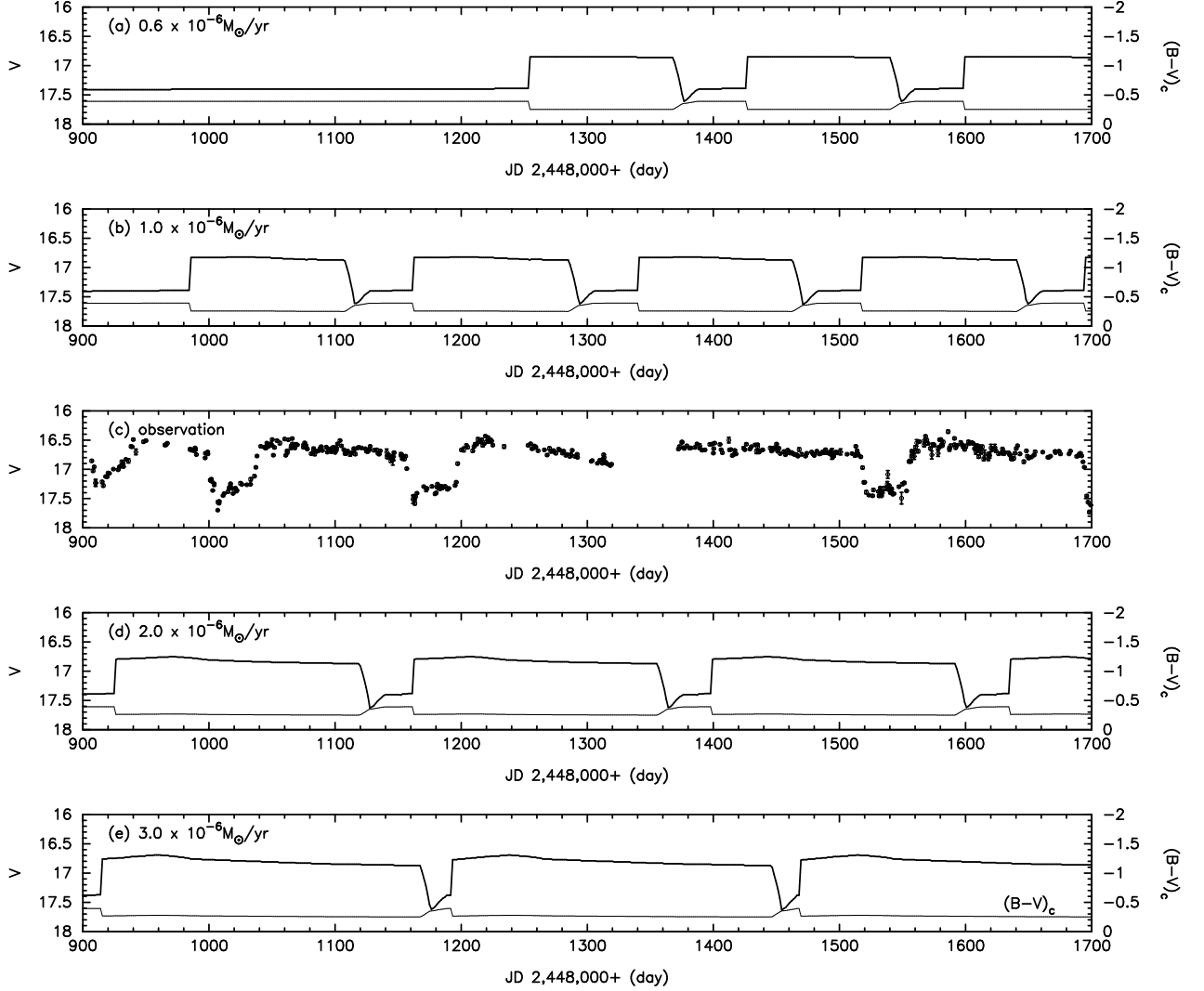


FIG. 8.— Calculated V -magnitude and $B - V$ color light curves are plotted against time (JD 2,448,000+) for our $M_{\text{WD}} = 1.1 M_{\odot}$ models. The model parameters are summarized in Table 1: (a) $\dot{M}_{\text{MS}} = 0.6 \times 10^{-6} M_{\odot} \text{ yr}^{-1}$, (b) $\dot{M}_{\text{MS}} = 1.0 \times 10^{-6} M_{\odot} \text{ yr}^{-1}$, (c) observational V -magnitudes (taken from Alcock et al. 1996), (d) $\dot{M}_{\text{MS}} = 2.0 \times 10^{-6} M_{\odot} \text{ yr}^{-1}$, (e) $\dot{M}_{\text{MS}} = 3.0 \times 10^{-6} M_{\odot} \text{ yr}^{-1}$. The other parameters of $c_1 = 10.0$ and $t_{\text{vis}} = 45.0$ days are common among the model light curves. We adopt the apparent distance modulus of $(m - M)_V = 18.7$.

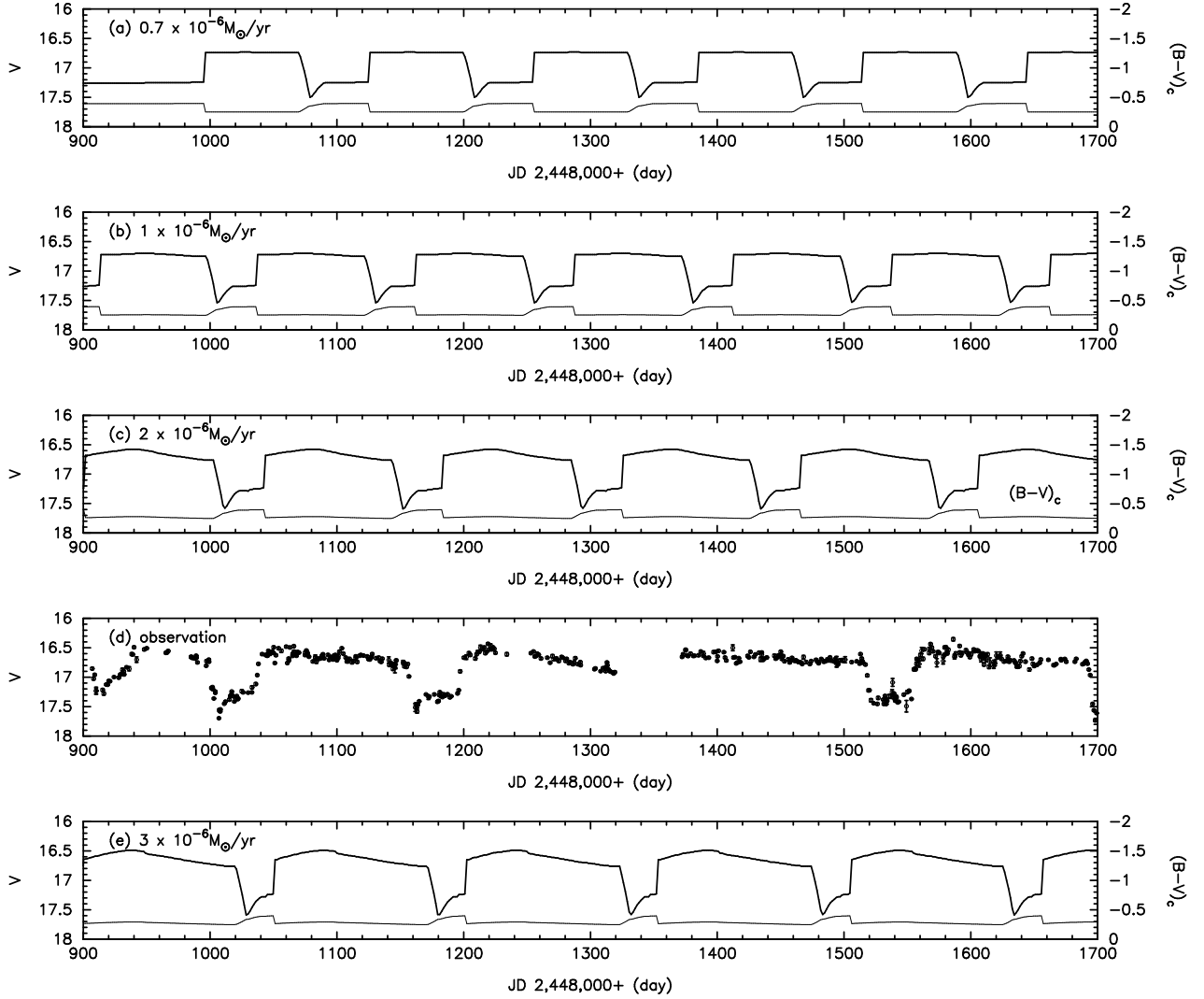


FIG. 9.— Calculated V -magnitude and $B-V$ color light curves are plotted against time (JD 2,448,000+) for a different value of $c_1 = 5.0$. The model parameters are summarized in Table 1: (a) $\dot{M}_{\text{MS}} = 0.7 \times 10^{-6} M_{\odot} \text{ yr}^{-1}$, (b) $\dot{M}_{\text{MS}} = 1.0 \times 10^{-6} M_{\odot} \text{ yr}^{-1}$, (c) $\dot{M}_{\text{MS}} = 2.0 \times 10^{-6} M_{\odot} \text{ yr}^{-1}$, (d) observational V -magnitudes (taken from Alcock et al. 1996), (e) $\dot{M}_{\text{MS}} = 3.0 \times 10^{-6} M_{\odot} \text{ yr}^{-1}$. The other parameters of $M_{\text{WD}} = 1.3 M_{\odot}$ and $t_{\text{vis}} = 36.0$ days are common among the model light curves. We adopt the apparent distance modulus of $(m - M)_V = 18.7$.

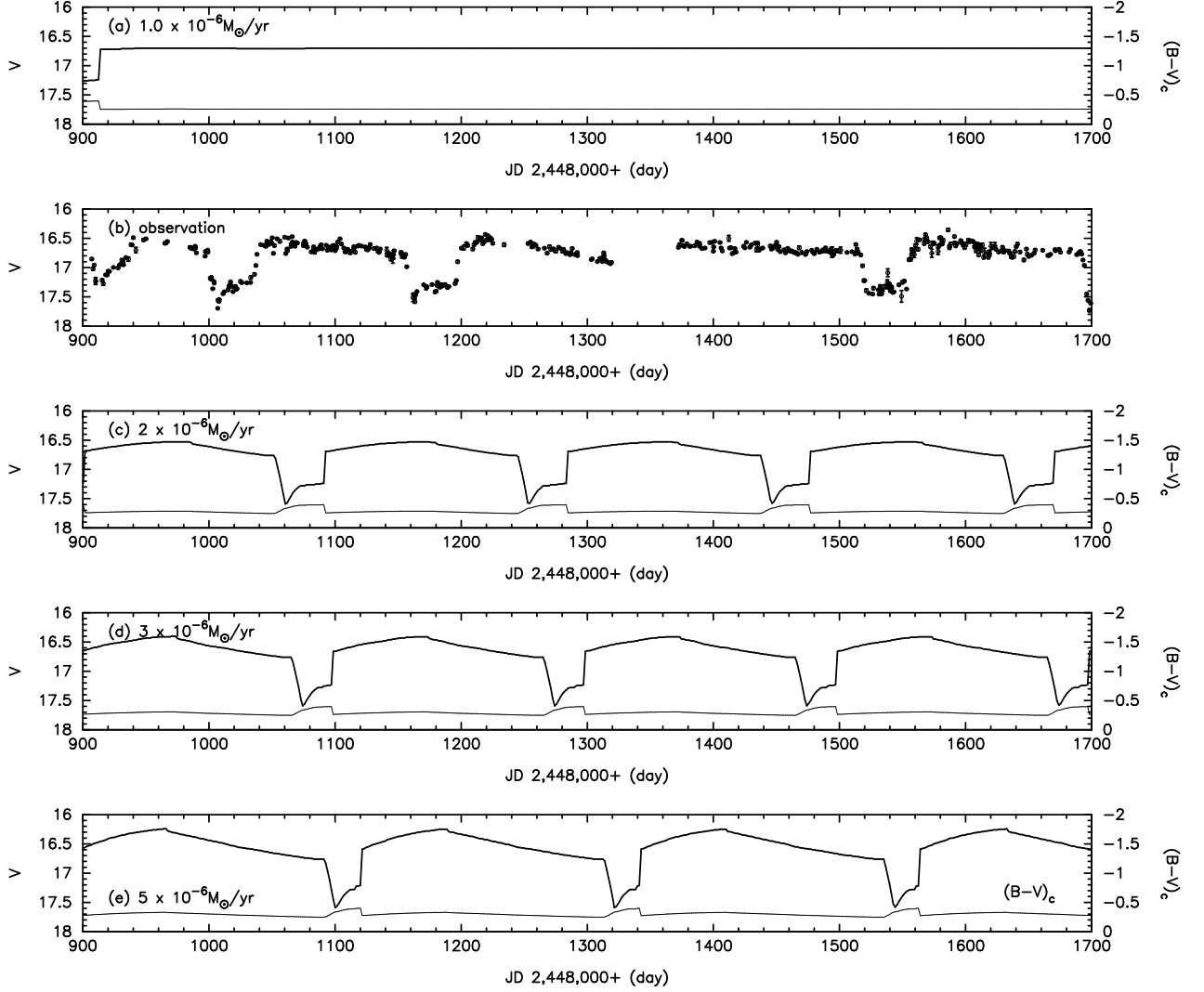


FIG. 10.— Calculated V -magnitude and $B - V$ color light curves are plotted against time (JD 2,448,000+) for a different value of $c_1 = 1.5$. The model parameters are summarized in Table 1: (a) $\dot{M}_{\text{MS}} = 1.0 \times 10^{-6} M_{\odot} \text{ yr}^{-1}$, (b) observational V -magnitudes (taken from Alcock et al. 1996), (c) $\dot{M}_{\text{MS}} = 2.0 \times 10^{-6} M_{\odot} \text{ yr}^{-1}$, (d) $\dot{M}_{\text{MS}} = 3.0 \times 10^{-6} M_{\odot} \text{ yr}^{-1}$, (e) $\dot{M}_{\text{MS}} = 5.0 \times 10^{-6} M_{\odot} \text{ yr}^{-1}$. The other parameters of $\dot{M}_{\text{WD}} = 1.3 M_{\odot}$ and $t_{\text{vis}} = 62.0$ days are common among the model light curves. We adopt the apparent distance modulus of $(m - M)_V = 18.7$.

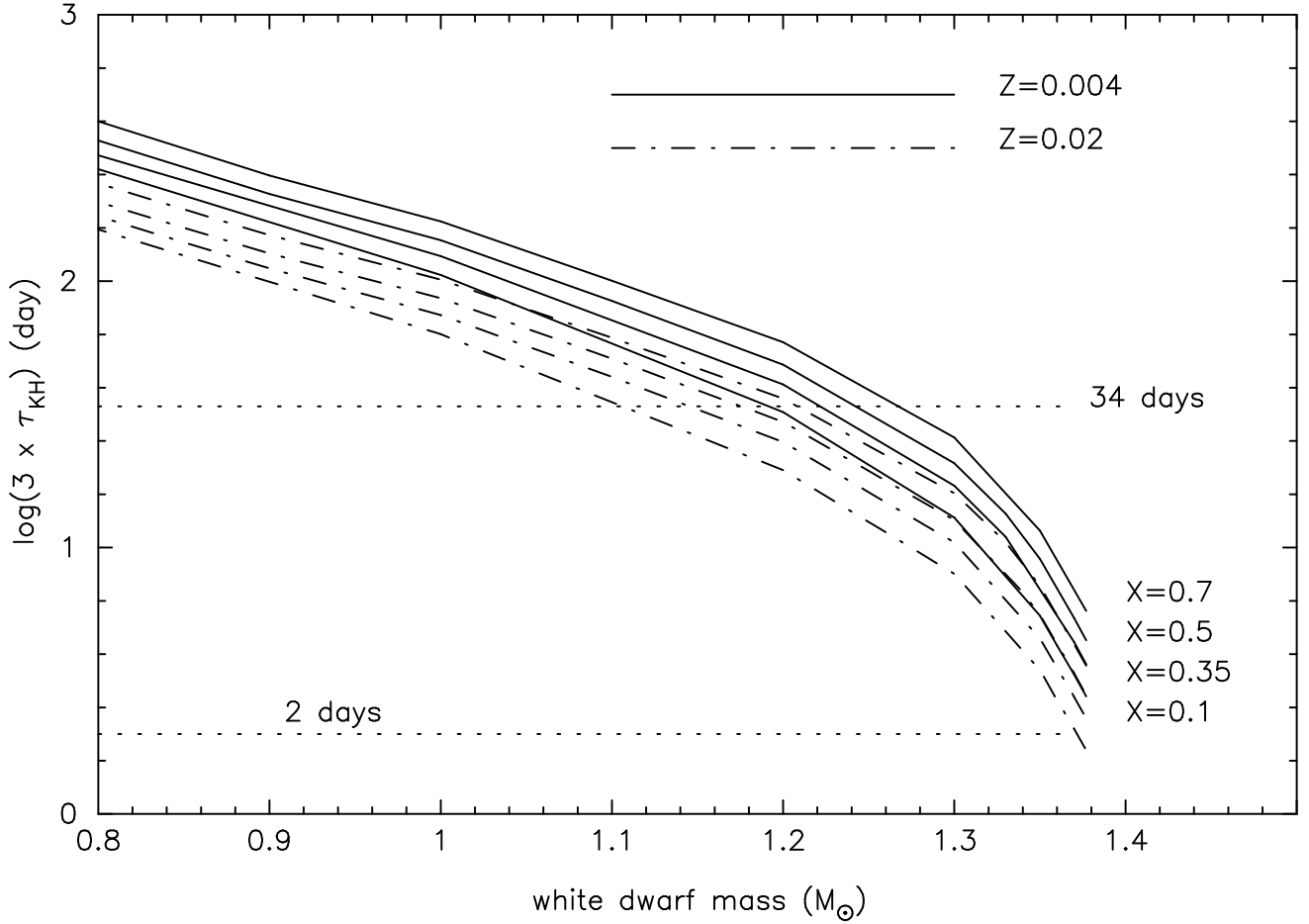


FIG. 11.— Three times the Kelvin-Helmholtz timescale of the WD envelope is plotted against the WD mass. Since the timescale depends on the metallicity (Z) and the hydrogen content (X), we plot four cases of the hydrogen content, $X = 0.1, 0.35, 0.5$, and 0.7 , number of which is attached to each line, each for two cases of the metallicity, $Z = 0.004$ (*solid line*) and $Z = 0.02$ (*dashed-dotted line*). Here we have calculated $\tau_{KH} = (\text{thermal energy of the WD envelope}) / (\text{luminosity of the WD})$ just after the wind stops. This corresponds to the shortest timescale that the WD photosphere shrinks by a factor of four, i.e., from $\sim 0.08 R_{\odot}$ ($\sim 25 \text{ eV}$) to $\sim 0.02 R_{\odot}$ ($\sim 50 \text{ eV}$).

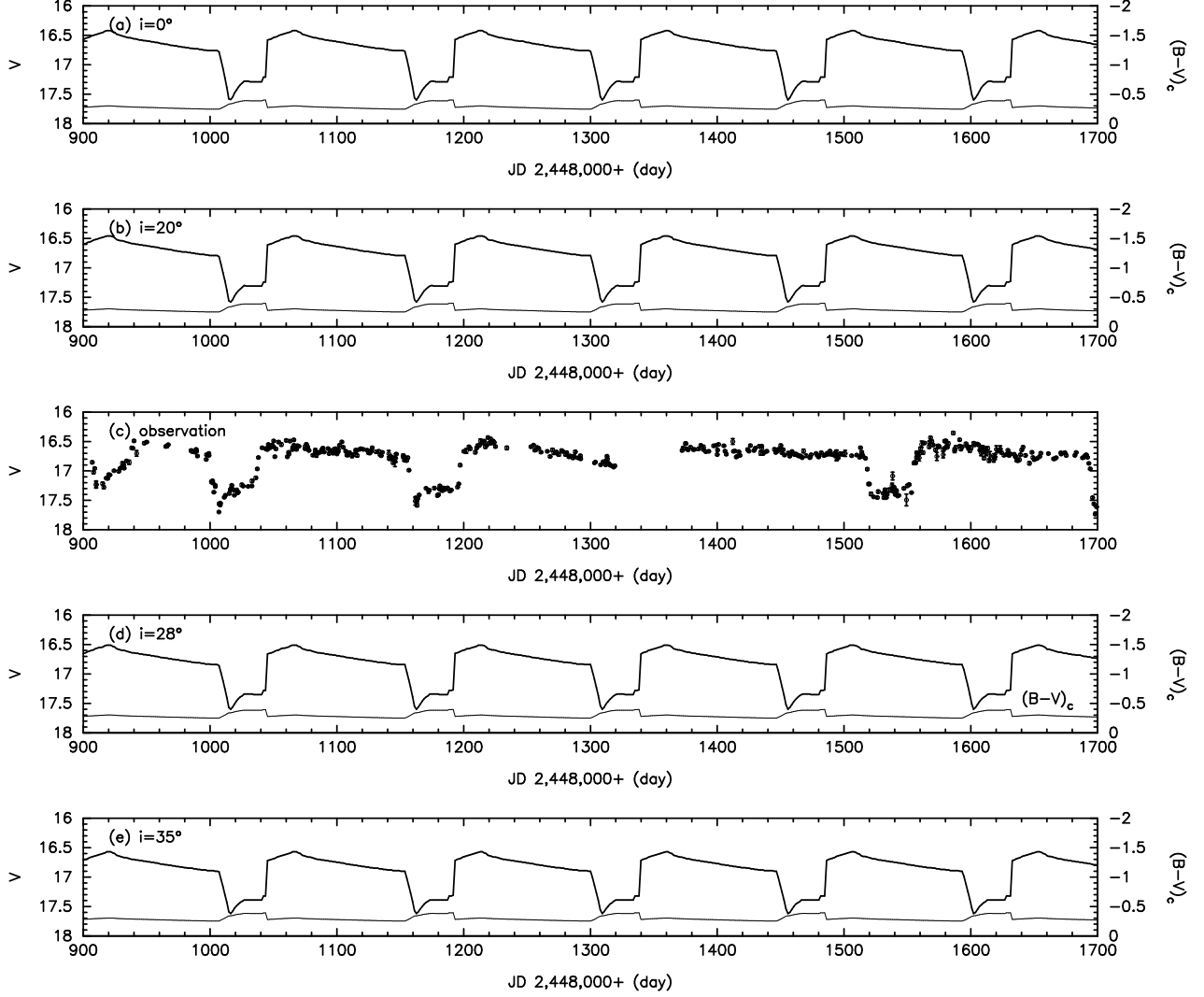


FIG. 12.— Calculated V -magnitude and $B - V$ color light curves are plotted against time (JD 2,448,000+) for various inclination angles of (a) $i = 0^\circ$, (b) $i = 20^\circ$, (c) MACHO observation taken from Alcock et al. (1996), (d) $i = 28^\circ$, and (e) $i = 35^\circ$. The other model parameters are the same as those in Fig. 4.

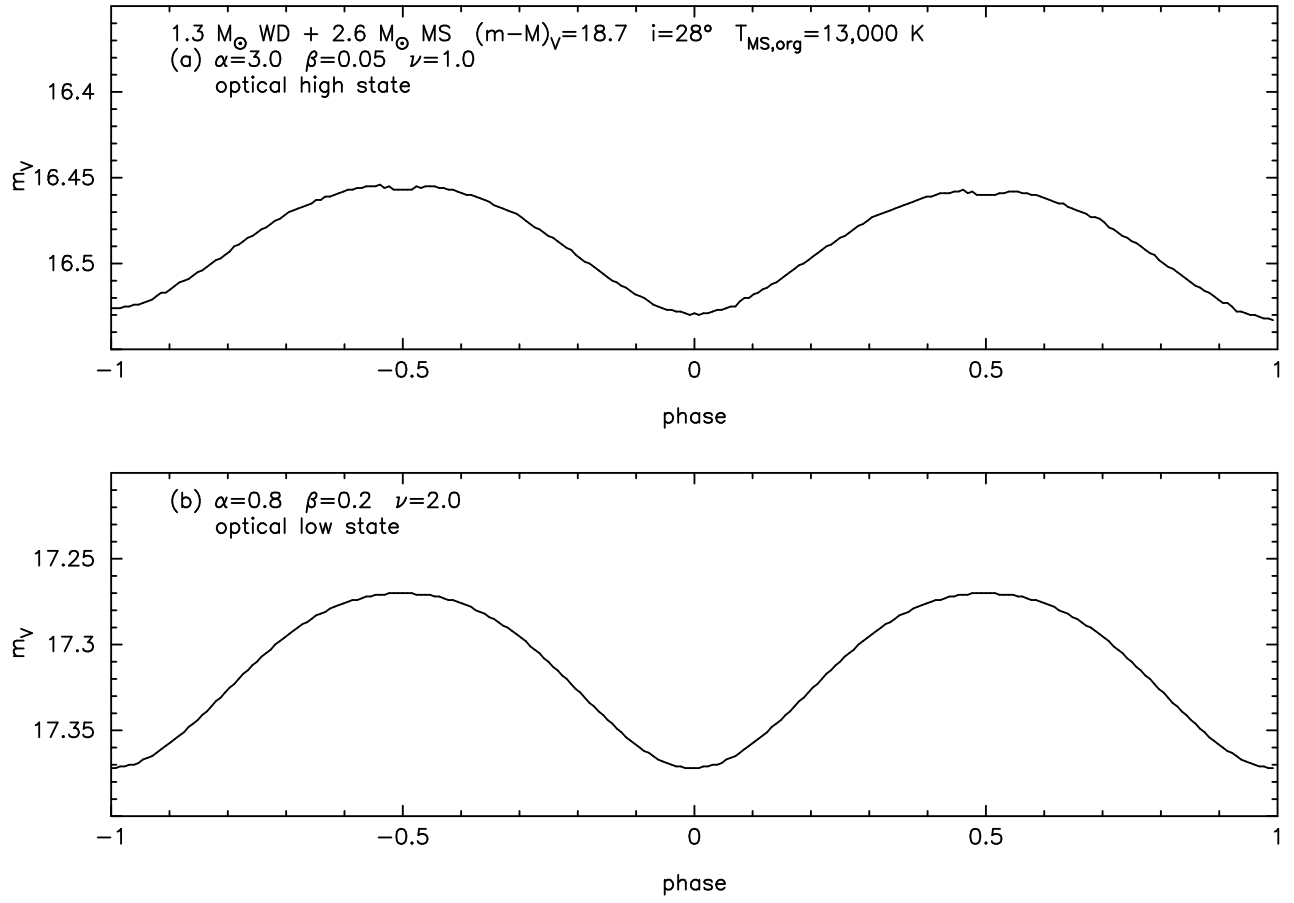


FIG. 13.— Calculated V -magnitudes are plotted against two orbital phases (from -1.0 to 1.0) for (a) the optical high state and (b) the optical low state. We adopt the inclination angle of $i = 28^\circ$. The other model parameters are the same as those in Fig. 4.